Heliyon 10 (2024) e32561

Contents lists available at ScienceDirect

Heliyon

journal homepage: www.cell.com/heliyon

Research article

Development and validation of an oil palm model for a wide range of planting densities and soil textures in Malaysian growing conditions

Christopher Boon Sung Teh [a,*], See Siang Cheah [b], Harikrishna Kulaveerasingam [b]

[a] Faculty of Agriculture, Universiti Putra Malaysia, Malaysia
[b] Sime Darby Plantation Research Sdn. Bhd., Malaysia

ARTICLE INFO

Keywords:
Photosynthesis
Respiration
Water deficit
Water stress
Evapotranspiration
Tenera

ABSTRACT

A semi-mechanistic oil palm growth and yield model called Sawit.jl was developed to account for a wide range of planting densities and soil textures under Malaysia's climate conditions. The model comprises components related to meteorology, photosynthesis, energy balance, soil water content, and crop growth. The model simulates instantaneous meteorological properties using daily weather data, calculates simultaneous evaporation from crop and soil with the Shuttleworth-Wallace model, determines soil water content through Darcy's law, and adapts a biochemical C3 model for photosynthesis. The model is also parameterized using updated measurements from the newer tenera oil palm, including temperature-dependent Rubisco kinetics, specific leaf area, and the partitioning of nutrients and dry matter between various tree parts. Sawit.jl was validated using historical field measurement data from seven Malaysian oil palm sites, encompassing palm ages spanning 1–23 years. These seven sites differed in soil type (Inceptisols and Ultisols), planting density (82–299 palms ha^{-1}), soil texture (27–59 % clay and 7–67 % sand), and rainfall (1800–2800 mm yr^{-1}). The model showed overall good accuracy in simulating oil palm parameters (except for trunk weight) across diverse conditions, with model agreement metrics ranging from 6 to 27 % for model absolute errors, −22 to +17 % for model bias, and 0.38 to 0.98 for the Kling-Gupta Efficiency index. The model also predicted the response of oil palm yield to abrupt rainfall changes, such as those during El Niño and La Niña events, while accounting for how soil texture, rainfall, and other meteorological factors influence water deficits and crop photosynthesis. However, model accuracy varied by site, planting density, and oil palm parameter. Model accuracy can be increased by more accurately representing the oil palm microclimate, incorporating fruiting activity, and refining the dry matter partitioning mechanism for the trunk.

1. Introduction

Oil palm (*Elaeis guineensis* Jacq.) is the world's most important vegetable oil crop, surpassing soybean [1]. Malaysia is the second largest producer and exporter of palm oil worldwide, with 18 % of the country's total land area, or 5.87 million ha, covered by this single crop alone in 2020 [2,3].

* Corresponding author.
E-mail address: chris@upm.edu.my (C.B.S. Teh).

https://doi.org/10.1016/j.heliyon.2024.e32561
Received 25 May 2023; Received in revised form 2 June 2024; Accepted 5 June 2024
Available online 15 June 2024

Various factors influence oil palm growth, including the weather, soil, crop, and other environmental elements. Due to the complex relationship between these factors and the fact that oil palm is a sizable tree with a commercial lifespan of 20–30 years, interest in oil palm models has increased. These models can be used alongside or as alternatives to field trials, particularly when the trials are time-consuming, costly, or technically challenging, such as in certain climate change studies. Oil palm models allow for quick assessment of multiple factors affecting crop production and aid in developing adaptive crop management strategies, such as modifying planting densities, selecting cultivars, applying irrigation, devising fertilization methods, and planning crop rotations [4–6]. Oil palm models are useful tools for evaluating crop performance in various environments and management approaches. Rival [7] emphasized that developing climate-adaptive oil palm varieties requires a multidisciplinary approach, and that modeling oil palm responses to changing climatic conditions is crucial for establishing climate-resilient genotypes and farming practices.

OPSIM was the first semi-mechanistic model for oil palm growth and yield, and its introduction was significant [8]. It was the first to integrate crop physiology, physical processes, and the underlying relationships between the crop and its environment. Subsequent modifications were made to OPSIM to include more physical-based equations for photosynthesis [9]. Over the last four decades, several other oil palm models have emerged. These include SIMPALM, GPHOT and GPHOT2, OPLFSIM3, OPRODSIM, ECOPALM, PALMSIM, APSIM-Oil Palm, CLM-Palm, CLIMEX-Oil Palm, and ORCHIDEE–MICT–OP [10–20].

The primary goal of this study was to develop and validate a more mechanistic model for oil palm growth and yield, accounting for a wide range of planting densities and soil textures in Malaysia's climate conditions. The first objective was to improve the photosynthesis simulations by incorporating a more flexible and representative biochemical photosynthesis model for oil palm. Except for CLM-Palm and ORCHIDEE–MICT–OP, the current oil palm models utilize the radiation use efficiency function to relate intercepted radiation to the gross assimilates produced through photosynthesis. These functions are simple to formulate and use, but they are empirical and thus less reliable for simulating photosynthesis responses to various environmental factors [21]. In contrast, biochemical photosynthesis models, such as those developed by Farquhar et al. [22] and later adapted by Collatz et al. [23], are more physical based. As a result, these models are considered more versatile and accurate under diverse conditions [18,20,24,25]. However, they require more data, such as information on the temperature dependency of Rubisco kinetics, the maximum Rubisco carboxylation rate $V_{c,max}$, and the CO_2 photocompensation point [26]. Unfortunately, these parameters and their temperature dependencies are largely unknown for oil palm, although there have been several attempts to estimate $V_{c,max}$ for oil palm [18,20,27,28].

Second, this research aimed to improve evapotranspiration (ET) simulations by incorporating the microclimate conditions within oil palm canopies and the simultaneous evaporative water loss from both soil and tree. ET is a core component of the hydrological cycle and is directly related to crop water stress, soil water content, photosynthesis, and energy balance [29]. As such, the development and implementation of more precise and dependable ET simulations are of paramount importance. Some oil palm models use either the Penman-Monteith model or a simple transpiration efficiency (TE) coefficient to simulate ET [17,30]. These methods are inadequate for modeling the complex microclimate environment within the oil palm canopies. For instance, the TE coefficient is an empirical value that is likely to vary by season and location, as it depends on weather and management practices [31,32]. And the Penman-Monteith model only accounts for evaporative losses from the crop or soil, but not both concurrently. Evaporation from the soil, especially in the wide spacing of oil palm rows and beneath partially closed canopies, can be significant [33]. Overlooking this aspect may result in large errors when modeling low-density oil palm stands. The Shuttleworth-Wallace model extends the Penman-Monteith model to allow concurrent heat fluxes from soil and crop [34]. Since its introduction, this model has been used widely and has performed well [35–38]. However, to the best of our knowledge, this model has not yet been applied to oil palm research. However, like the Penman-Monteith model, the main limitation of the extended model is its parameterization, which remains largely unknown for oil palm.

The third aim was to update the model with data on higher-yielding tenera oil palms instead of older dura materials, particularly on the partitioning of 1) nitrogen and mineral content, and 2) dry matter in individual tree parts. Many oil palm models employ respiration coefficients to simulate the maintenance respiration. These coefficients are calculated based on the nitrogen and mineral content in different tree parts, thereby making this method more mechanistic or physical-based [39,40]. However, these coefficients were derived either from a single tenera × dura (L2T × D10D) oil palm progeny grown on the Ivory Coast (*e.g.*, SIMPALM and PALMSIM) or from measurements by Ng et al. [41], who sampled older dura oil palms in good growing conditions in Malaysia (*e.g.*, OPSIM and OPRODSIM). However, these maintenance respiration coefficients may not be accurate today, as they originate from outdated planting materials instead of the current high-yielding tenera. Oil palm growth can be divided into vegetative growth (leaf, trunk, and root) and reproductive growth [42]. The techniques used to simulate vegetative growth are primarily empirical and are based on the vegetative dry matter requirement or phytomer phenology of the oil palm [8,10,14,15,18,20,43]. Therefore, using updated measured data from the current tenera oil palm would enable a more accurate representation of the growth dynamics of the oil palm.

The final aim was to develop a model applicable to a wider range of planting densities, acknowledging that planting density strongly affects oil palm growth and yields [44–47]. Many commercial oil palm plantations generally have between 128 and 148 palms ha^{-1}, but a wide range of planting densities have been explored in attempts to increase oil palm yield [44,45,48–50]. Changes in planting density will affect the interception of solar irradiance, the microclimate within oil palm canopies, and soil water balance. Except for OPRODSIM, the present oil palm models are only applicable to a narrow range of planting densities.

To develop this oil palm model, results from several of our works were used to parameterize the model, including hourly simulations of meteorological properties, parameterization of the biochemical model of C3 leaf photosynthesis, and determination of the maintenance respiration coefficients and dry matter partitioning between various tree parts [51–53]. Specifically, our work included the validation of hourly weather simulations for six major oil palm growing areas in Malaysia from 2015 to 2017 and the parameterization of the Farquhar-von Caemmerer-Berry C3 photosynthesis model specifically for oil palm, in which six replicates from palm ages of 7 months and 1, 2, 7, and 12 years were measured [52,53]. Finally, we quantified the standing biomass, dry matter production,

and nutrient demand of oil palm aged 1, 2, 4, 7, 11, 17, and 20 years [51]. All these works represented Malaysian conditions, where the current tenera oil palm was planted and grown under current agronomic practices in Malaysia. Model simulations were validated against historical field measurement data from different palm ages (1–23 years) in seven oil palm plantations across Peninsular Malaysia, growing under various soil textures, weather conditions, and a wide range of planting densities (82–299 palms ha^{-1}).

2. Model development

2.1. General framework

An oil palm model called *Sawit.jl* was coded in the Julia programming language [54]. It simulates the growth and yield of individual oil palm stands, specifically for crop production level 2, where growth is constrained only by climate and water availability [55]. The model assumes an optimal nutrient level for the oil palm and does not consider the effects of pests, diseases, or weeds. It also presumes standard management practices, such as pruning and mulching, as is typically observed in Malaysia's oil palm industry.

The model comprises six core components: 1) the main loop, 2) meteorology, 3) photosynthesis, 4) energy balance, 5) soil water, and 6) crop growth (Fig. 1). A simulation run starts with the main loop. It initializes the model state by reading the input data from a file and then transfers the control to the meteorology component. Utilizing daily weather data, this component calculates instantaneous meteorological properties, including air temperature, wind speed, solar irradiance, air vapor pressure, and relative humidity. The global model state is then updated with this new information.

The photosynthesis and energy balance components next compute the radiation regime in oil palm canopies and resolve the energy balance of the system. They calculate the energy partitioning, wind speed profile, and resistances to determine the evaporative water

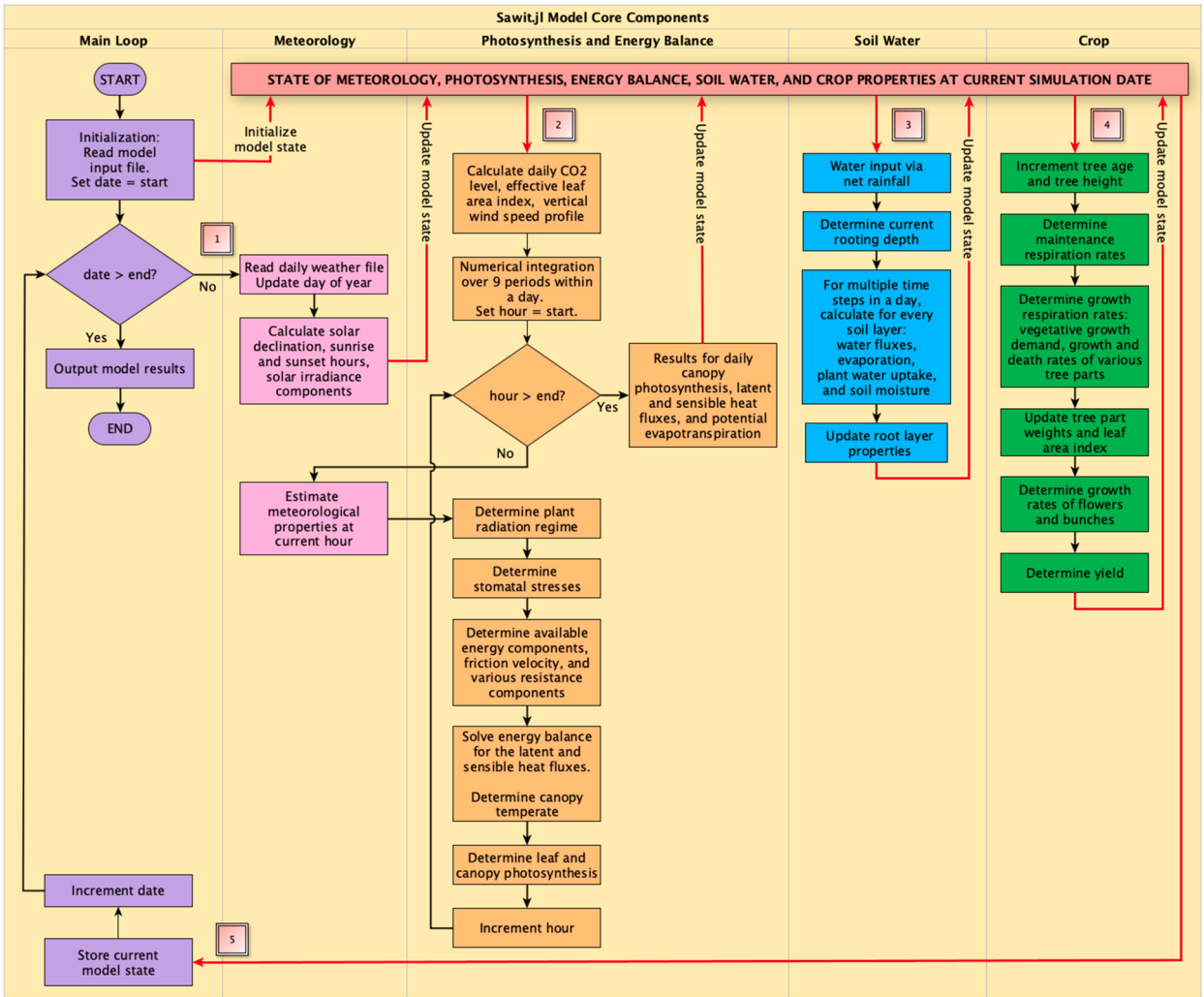

Fig. 1. General framework of Sawit.jl model. The numbers in squares represent the primary model routes or paths, where the simulation sequentially cycles through paths 1 to 5 and then repeats from 1 until it ends.

losses and canopy temperature. These factors are essential for computing oil palm photosynthesis while considering the constraints of water, solar radiation, and air vapor pressure deficit.

After updating the global model state, the soil water component calculates the soil water content by dividing the soil profile into several layers and then solving the one-dimensional water fluxes within each layer. The net water flux is the daily change in soil water content, which is the difference between incoming and outgoing water fluxes. As before, the global model state is then updated.

Finally, the crop component calculates the maintenance and vegetative growth respiration rates to determine the assimilate allocation from photosynthesis for crop maintenance, growth, bunch production, and yield. It also computes the daily increase in tree height and rooting depth. The daily results are saved to an output file, and the main loop advances the simulation date. Simulation ends when the current date surpasses the specified end date.

2.2. Meteorology component

The site's local solar hours of sunrise t_{sr} and sunset t_{ss}, day length (h), solar inclination (rad), extraterrestrial solar irradiance I_{et} (W m^{-2}), relative humidity RH (%), and air vapor pressure (mbar) were determined from Ephrath et al. [56], and Goudriaan and van Laar [57]. Instantaneous meteorological properties, such as direct and diffuse solar irradiance, wind speed, air temperature, vapor pressure, and humidity, were estimated based on the daily measured meteorological parameters of minimum and maximum air temperature (°C) and wind speed (m s^{-1}). Daily measured rainfall data were also required.

Total solar irradiance I_t consists of two components: the direct (beam) component I_{dr} and the diffuse component I_{df}. The direct component arrives from a single source (the position of the sun), whereas the diffuse component arrives from all directions as a result of scattering and reflection on various surfaces. The partitioning of I_t into I_{df} and I_{dr} was based on calculations by Khatib et al. [58], who fitted Eq. (1) to 20-year daily solar radiation data from 28 sites across Malaysia to obtain

$$I_{df} / I_t = 0.9505 + 0.91634K_T - 4.851K_T^2 + 3.2353K_T^3 \quad (1)$$

where K_T is the sky clearness index, which is simply the ratio between I_t and I_{et}. Following the method by Dimas et al. [59], K_T was estimated from RH by fitting a linear function between the measured hourly values from five oil palm sites in Malaysia (Fig. 2) [52]. The daily solar irradiance components of direct $I_{dr,d}$ and diffuse $I_{df,d}$ were calculated by integrating the instantaneous solar irradiance components of direct I_{dr} and diffuse I_{df}, respectively, from sunrise t_{sr} to sunset t_{ss}.

The daily trend of air temperature was described by the set of equations given by Wilkerson et al. [60], in which air temperature varied sinuously with time between 1.5 h after the time of minimum air temperature and the time of sunset. For periods outside of this period, the air temperature declined linearly with time.

Similarly, instantaneous wind speed was also assumed to vary sinuously between 1.5 h after sunrise and sunset [56]. Outside this period, wind speed was assumed to be constant at a minimum value, as described by $u_{\min}$. The daily wind speed trend was estimated using Eq. (2a):

$$u = u_{min} + (u_{max} - u_{min})\, sin[\pi(t_h - t_{sr} - 1.5)/DL]; \quad u \geq u_{min} \quad (2a)$$

where u is the wind speed at a given local solar hour (m s^{-1}); t_h is the local solar hour; and $u_{\max}$ and $u_{\min}$ are the maximum and minimum wind speeds for the day, respectively (m s^{-1}). The mean daily minimum and maximum wind speeds were estimated by fitting the following empirical equations (Eq. 2 b-c) to the measured 10-year wind speed data from several towns in Malaysia:

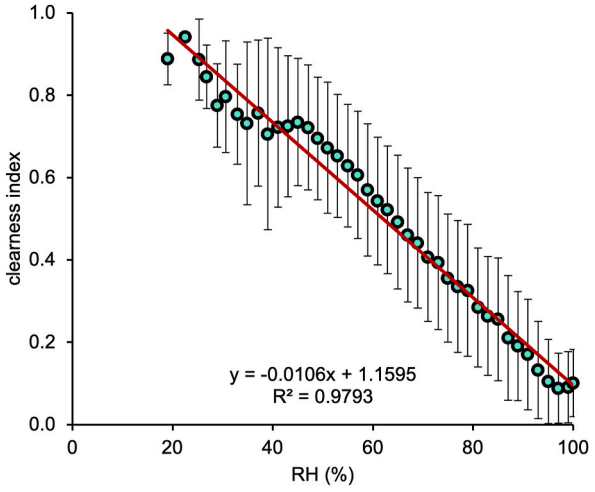

Fig. 2. Linear relationship between mean relative humidity (RH) and mean sky clearness index for five sites in Malaysia (N = 25,548) [52]. Bars represent ±1 SD.

$$u_{min} = 0.5591 u_d^{1.25} \quad (2b)$$

$$u_{max} = 1.7976 u_d^{0.75} \quad (2c)$$

where u_d is the mean measured daily wind speed (m s^{-1}) [61].

2.3. Photosynthesis component

2.3.1. Plant radiation regime

The plant radiation regime within canopies comprises four solar radiation flux components [62]. These four components include the unintercepted direct radiation with and without the addition of scattered beams, the sole scattered component, and the average diffuse solar radiation. The ability of canopies to intercept solar radiation was measured using the canopy extinction coefficient for direct and diffuse components. Oil palm canopies were assumed to be randomly distributed in the aerial space so that the canopy extinction coefficient for direct radiation k_{dr} could be determined from Goudriaan [63]. To account for partially closed canopies, the k_{dr} for full canopies was adjusted by multiplying it by a canopy clustering coefficient ω, following Campbell and Norman [62] to give $k_{dr} \bullet \omega$, such that ω ranges from 1 for fully closed canopies to 0 for the absence of canopies. Following the approach by Teh [64], the canopy extinction coefficient for diffuse radiation k_{df} was derived by integrating $k_{dr} \bullet \omega$ over a uniform overcast sky, as defined by Lemeur and Blad [65], and over the whole canopy from 0 to L (leaf area index; m^2 leaf m^{-2} ground) to obtain Eq. (3) as follows:

$$k_{df} = exp\left(0.25 - 0.52\sqrt{L}\right) \quad (3)$$

The interception of solar radiation accounts for the reflection (albedo) from the canopies and the soil surface [57,63].

The oil palm canopy was divided into two parts: sunlit and shaded. The sunlit canopy is a part of the canopy that is exposed to the direct radiation of Q_{sl} and has a total leaf area of L_{sl} (sunlit leaf area index). Similarly, the shaded canopy is the part that is exposed to the diffuse radiation of Q_{sh} and has a total leaf area of L_{sh} (shaded leaf area index). This means that the total leaf area index L of the whole canopy is the sum of L_{sl} and L_{sh} (all in m^2 leaf m^{-2} ground). Calculations for Q_{sl}, Q_{sh}, L_{sl}, and L_{sh} were determined from Goudriaan and van Laar [57], and Campbell and Norman [62].

2.3.2. CO_2 assimilation

Oil palm canopy CO_2 assimilation was determined using Eq. (4), following the method of Collatz et al. [23], which is an adaptation of the model by Farquhar et al. [22]. Gross leaf CO_2 assimilation rate Λ (μmol CO_2 m^{-2} leaf s^{-1}) was taken as the lowest of the three assimilation rates limited by Rubisco, light, and sink:

$$\Lambda = MIN\left[v_c, \left(v_{q,sl} + v_{q,sh}\right), v_s\right] \quad (4)$$

where v_c, $v_{q,sl/sh}$, and v_s are the assimilation of CO_2 limited by Rubisco, light, and sink, respectively; and the *MIN* is a function to select the minimum of the given values. One important parameter in the calculations of the Rubisco- and light-limited assimilation rates is the intercellular CO_2 concentration C_i (μmol mol^{-1}), which is related to the ambient CO_2 concentration C_a (μmol mol^{-1}), following Yin et al. [66], as follows:

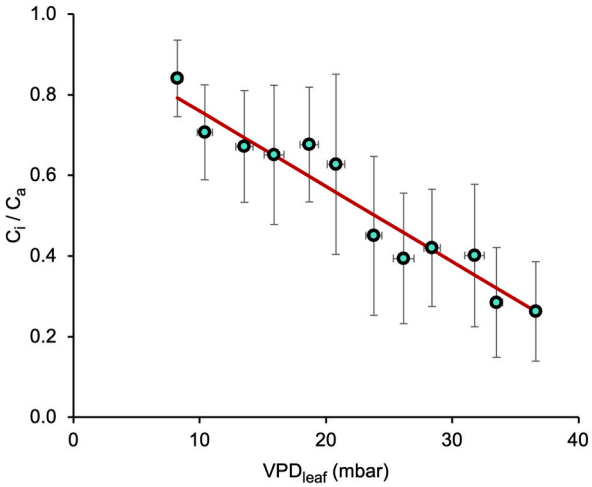

Fig. 3. Linear decline in the mean ratio between intercellular (C_i) and ambient (C_a) CO_2 concentrations with increasing mean leaf vapor pressure deficit (VPD_{leaf}) for oil palm trees aged 1–19 years (N = 654) [53]. Leaf gas exchange was measured based on Long and Bernacchi [67] using the TPS-2 Portable Photosynthesis System (PP Systems International, Inc., Amesbury, US). Bars represent ±1 SD.

$$C_i / C_a = 1 - (1 - \Gamma^* / C_a)(a + b \times VPD_{leaf}) \quad (5)$$

where Γ*, determined from Collatz et al. [23], is the CO_2 compensation point (mbar), which is the CO_2 concentration at which the rate of photosynthesis is equal to the rate of respiration; and VPD_{leaf} is the leaf vapor pressure deficit (mbar), which is the difference between the saturated air vapor pressure at canopy temperature T_f and the ambient air vapor pressure. The coefficients a and b in Eq. (5) were determined by Cheah and Teh [53] as 0.0615 and 0.0213, respectively (Fig. 3).

Calculations for the Rubisco-, light- and sink-limited assimilation rates and their respective parameters were from Collatz et al. [23]. However, the values of several of these photosynthetic parameters (Table 1) depended on canopy (foliage) temperature T_f (°C), so each of these parameters was corrected using the Arrhenius equation, given by Eq. (6) as follows:

$$\xi = \xi_{(25)} \times Q_{10,\xi}^{(T_f - 25)/10} \quad (6)$$

where ξ and $\xi_{(25)}$ are the parameter values after temperature correction and at 25 °C, respectively; and $Q_{10,\xi}$ is the relative change in the parameter ξ for every 10 °C change (their values as listed in Table 1).

The maximum Rubisco carboxylation rate at 25 °C or $V_{c,max(25)}$ for oil palm was measured by Cheah and Teh [53] for tree ages 7 months to 12 years, and its relationship with tree age (in days) can be described by

$$V_{c,\max(25)} = exp[4.7971 - 0.9095\, exp(-age / 365)] \quad (7)$$

where $V_{c,max(25)}$ increased rapidly within the first two years, after which it gradually plateaued at a mean (±SD) of 120 ± 32 μmol m^{-2} s^{-1} at palm age 5 (Fig. 4). This mean maximum value for $V_{c,max(25)}$ is 20 % higher than the constant value of 100.7 μmol CO2 m^{-2} leaf s^{-1} given by Fan et al. [18], who derived this value from the leaf nitrogen content and specific leaf area for crops in general, not specifically oil palm leaves. The Rubisco enzyme will denaturate at high temperatures, and data from Cheah and Teh [53] projected the onset of Rubisco degradation to start at 46 °C. Consequently, $V_{c,max}$, calculated using Eq. (7), was first corrected for the current foliage temperature (Eq. (6)), then for high temperatures using Eq. (8) as follows:

$$V_{c,\max} = \left\{ V_{c,\max\ (25)} \times 2.532^{(T_f - 25)/10} \right\} \Big/ \left\{ 1 + \exp\left[0.2(T_f - 46)\right] \right\} \quad (8)$$

The gross leaf CO_2 assimilation rates were separately determined for sunlit and shaded leaves, then scaled up to gross canopy CO_2 assimilation (Λ_{canopy}; μmol CO_2 m^{-2} ground s^{-1}) by multiplying them with their respective leaf area indices, L_{sl} and L_{sh} [62]. Daily gross canopy photosynthesis was finally determined by integrating Λ_{canopy} from sunrise t_{sr} to sunset t_{ss}.

2.4. Energy balance component

Shuttleworth and Wallace [34] extended the Penman-Monteith model by Monteith [30] to enable the simultaneous evaporative losses from both crop and soil. They modeled the energy balance of the soil-plant-atmosphere system as a network of aerodynamic and surface resistances, in which heat fluxes must traverse within the system. The entire soil-plant-atmosphere system was described by a series of eight independent equations, with eight unknown variables. Therefore, through algebraic manipulations, these equations can be solved to give the total potential latent λET and sensible H heat fluxes (all in W m^{-2}), as well as the air vapor pressure deficit at the mean canopy flow VPD_0 (mbar) [34,64]. In particular, knowing λET and VPD_0 would solve the partitioning of potential latent and sensible heat fluxes to the soil and crop, and solving for the crop sensible heat would allow the canopy temperature T_f (°C) to be known in subsequent photosynthesis calculations. The instantaneous latent heat fluxes were integrated over the entire day to determine the daily potential latent heat fluxes, which were then converted to the daily potential amount of water transpired (by plants) and evaporated (by soil), following Goudriaan and van Laar [57].

2.4.1. Available energy

The available energy for the soil-plant-atmosphere system is driven by net radiation R_n (W m^{-2}), which is the sum of incoming shortwave and net long-wave radiation, or

$$R_n = (1 - p) I_t + R_{nL} \quad (9)$$

where ρ is the surface albedo (0.15); and R_{nL} is the net long-wave radiation (W m^{-2}), determined from Brutsaert [72] and Ortega-Farias

Table 1
Parameter values for oil palm photosynthesis calculations. Parameters with subscript (25) denote their values at 25 °C. The Michaelis-Menten (MM) constants were from Bernacchi et al. [68,69] for general C3 plants. Other parameters were based on the oil palm leaf measurements by Cheah and Teh [53].

$\xi_{(25)}$	Description	Value	$Q_{10,\xi}$
$K_{c(25)}$	MM constant for CO_2 (μmol mol^{-1})	270	2.786
$K_{o(25)}$	MM constant for O_2 (μmol mol^{-1})	165,000	1.355
$\tau_{(25)}$	CO_2/O_2 specificity factor (μmol μmol^{-1})	2389	0.700
$V_{c,max(25)}$	Maximum Rubisco capacity rate (μmol m^{-2} s^{-1})	Varies with palm age	2.532

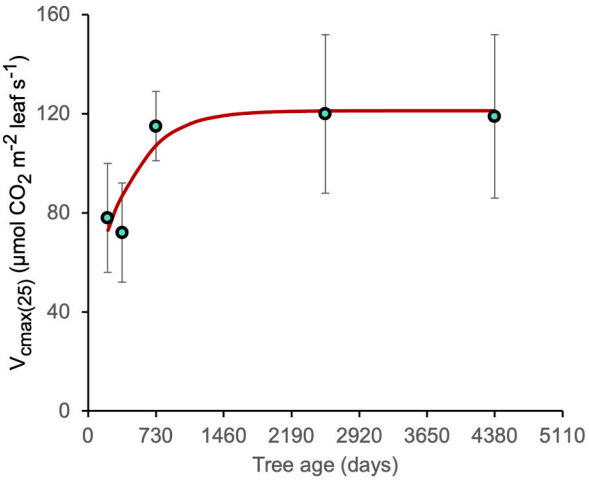

Fig. 4. Mean (±1 SD) changes in the maximum Rubisco capacity rate $V_{c,max(25)}$ with oil palm tree age [53]. Leaf gas exchanges for 7-month to 12-yr palm trees were measured (with 4–6 trees per age group) based on Long and Bernacchi [67] using the LI-6800-01 A portable photosynthesis system equipped with a Multiphase Flash fluorometer (Li-Cor Inc., Lincoln, NE, US). Then, based on the gas exchange data, $V_{c,max(25)}$ was estimated following Sharkey [70] and Sharkey et al. [71].

et al. [73]. Net radiation (Eq. (9)), after accounting for soil heat flux G (W m^{-2}), was then partitioned for crop and soil, following Shuttleworth and Wallace [34], and Goudriaan and van Laar [57]. The ratio of soil heat flux to net radiation (G/R_n) was set at 0.30 for sparse canopies, 0.07 for dense canopies, and subsequently adjusted based on the current leaf area index [30,74,75].

2.4.2. Vertical wind speed profile

Calculations of wind speed at any height require information on the zero-plane displacement height d (m) and crop roughness length z_0 (m) [34]. However, the values of these two parameters are uncertain for oil palm, but they can be estimated using Eqs. (10)–(13), given by Massman [76], as follows:

$$d = hZ \tag{10}$$

$$z_0 = h(1 - Z)exp(-k / U)to \tag{11}$$

$$Z = 1 - 0.5\ exp(-2\alpha_w)[exp(-2\alpha_w) - 1] / \alpha_w; \quad 0.30 \le Z \le 0.95 \tag{12}$$

$$U = 0.32 - 0.264\ exp\left(-15.1 C_d L_{eff}\right) \tag{13}$$

where α_w is the vertical wind speed extinction coefficient; h is the tree height (m); k is the von Karman constant (0.4); C_d is the foliage drag coefficient (0.2); and L_{eff} is the effective leaf area index (m^2 leaf m^{-2} ground), determined from Szeicz and Long [77] as follows:

$$L_{eff} = MIN[L, L_{max.PD} / 2] \tag{14}$$

where $L_{max,PD}$ is the maximum leaf area index (m^2 leaf m^{-2} ground) for a given planting density, PD (palms ha^{-1}). $L_{max,PD}$ (Eq. (14)) for oil palm was determined by fitting the best function (Eq. (15)) to the observed data by Cheah et al. [51]:

$$L_{max,PD} = 1.4119 + 0.0267PD \tag{15}$$

Vertical wind speed extinction coefficient α_w in Eq. (12), assumed equal to that for eddy diffusivity α_n, increases with L_{eff} per Massman [78] simulations on hypothetical plant stands (Eq. 16a-b):

$$\alpha_w = \alpha_n = 1/y \tag{16a}$$

$$y = -0.146 + 0.319/\sqrt{C_d L_{eff}}; \quad y \ge 0.2 \tag{16b}$$

2.4.3. Flux resistances

Heat fluxes must traverse various resistances within the soil-plant-atmosphere system, such as the resistances between the soil surface and mean canopy flow r_a^s and between the mean canopy flow and reference level r_a^a, bulk boundary layer resistance r_a^c, and canopy resistance r_s^c (all in s m^{-1}). The first three resistances were determined using Eqs. (17)–(19), given by Campbell and Norman [62], and Kustas and Norman [75] as follows:

$$r_a^s = exp(\alpha_n)\left[exp\left(-\alpha_n\frac{z_{s0}}{h}\right) - exp\left(-\alpha_n\frac{z_0+d}{h}\right)\right] / (\alpha_n k u_*) \quad (17)$$

$$r_a^a = ln\left(\frac{z_r-d}{h-d}\right) / (ku_*) + \left\{exp\left[n\left(1-\frac{z_0+d}{h}\right)\right] - 1\right\} / (\alpha_n k u_*) \quad (18)$$

$$r_a^c = \alpha_w\left\{0.01L_{eff}[1-exp(-0.5\alpha_w)]\sqrt{u_h/w}\right\}^{-1} \quad (19)$$

where z_{s0} is the soil surface roughness length (m), where for flat and tilled land, its value is 0.004 m, following Hansen [79]; and w is the mean pinnae width (m), determined using Eq. (20), which was derived by fitting the best function to the measured changes in leaf dimensions with oil palm tree age (in days) from Roa et al. [80], as follows:

$$w = 0.0152\ ln(age/365) + 0.0165 \quad (20)$$

The methods by Choudhury and Monteith [81], and Farahani and Ahuja [82] were used to determine the soil surface resistance r_s^s (s m^{-1}) (Eq. (21a)) as follows:

$$r_s^s = \tau_t l \bullet exp\left(-\frac{1}{\lambda}\times\frac{\theta_1}{\theta_{s,1}}\right) / (\varphi_p D_{m,v}) \quad (21a)$$

where $D_{m,v}$ is the vapor diffusion coefficient in air (24.7×10^{-6} m^2 s^{-1}); φ_p is the soil porosity (unitless); l is the dry soil layer thickness (taken as the first soil layer thickness) (m); θ_1 is the soil water content of the first soil layer (m^3 m^{-3}); $\theta_{s,1}$ is the saturated soil water content (m^3 m^{-3}) in the first soil layer; and λ is the soil pore-size distribution index (unitless), which can be estimated from the slope of the logarithmic suction-soil moisture curve, following Farahani and Ahuja [82]. τ_t in Eq. (21a) is the soil tortuosity (unitless), determined using Eq. (21b) from Shen and Chen [83] as follows:

$$\tau_t = \sqrt{\varphi_p + 3.79(1-\varphi_p)} \quad (21b)$$

Canopy resistance r_s^c (s m^{-1}) was determined by Eq. (22a):

$$r_s^c = 1 / (gst \times L_{eff}) \quad (22a)$$

where gst is the leaf stomatal conductance (m s^{-1}), which is the reduction in maximum leaf stomatal conductance gst_{max} (m s^{-1}) (Eq. (22b)) by low photosynthetically active radiation (PAR) f_{PAR}, plant water stress f_{water}, and high vapor pressure deficit (VPD) f_{VPD}:

$$gst = gst_{max} \times f_{PAR} \times f_{water} \times f_{VPD} \quad (22b)$$

where gst_{max} is 500 mmol m^{-2} s^{-1} or 0.012077 m s^{-1} for oil palm [84].

Each of these factors, f_{PAR}, f_{water}, and f_{VPD}, was scaled from 0 to 1; therefore, under optimal conditions, all three are equal to 1, resulting in gst being maximum at gst_{max}. Therefore, these factors quantify the severity or extent of non-optimal conditions. Following Kropff [85], f_{water} evaluates the intensity of water-limited conditions by calculating the disparity between the actual transpiration ET_c (m day^{-1}) and potential transpiration PET_c (m day^{-1}) as follows:

$$f_{water} = ET_c / PET_c \quad (23)$$

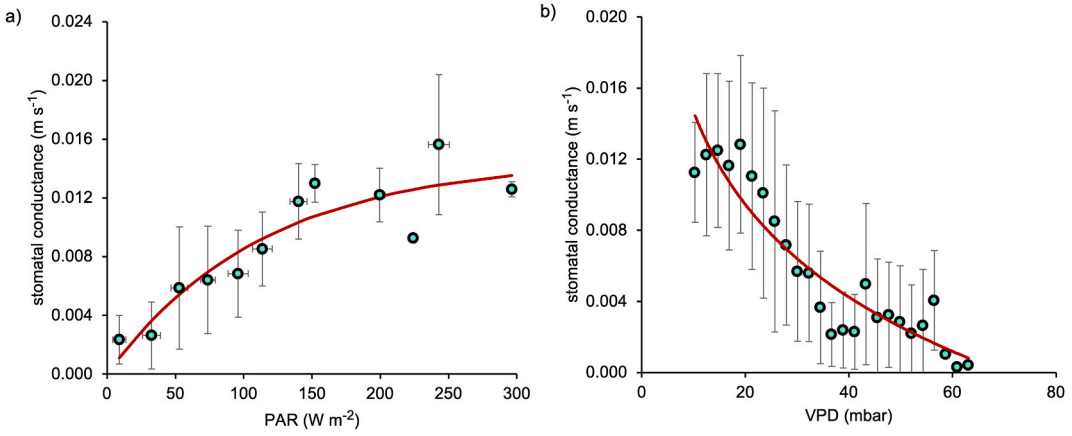

Fig. 5. Relationship between mean leaf stomatal conductance of oil palm with mean photosynthetically active radiation (PAR) (N = 381) (a) and mean air vapor pressure deficit (VPD) (N = 2591) (b) [53]. Leaf measurements were performed on 1- to 20-yr oil palm trees. Bars represent ±1 SD.

The factors f_{PAR} and f_{VPD} were determined by curve-fitting the measured data from Cheah and Teh [53] (Fig. 5a and b) to obtain Eq. 24a-b and 25a-b as follows:

$$f_{PAR} = gst[\![PAR]\!] / gst[\![PAR_{max}]\!] \tag{24a}$$

$$gst[\![PAR]\!] = 0.014614[1 - exp(0.00874PAR)] \tag{24b}$$

$$f_{VPD} = gst[\![VPD]\!] / gst[\![VPD_{min}]\!] \tag{25a}$$

$$gst[\![VPD]\!] = 0.0044272 - 0.01111\ ln(VPD) \tag{25b}$$

The functions $gst[\![PAR]\!]$ and $gst[\![VPD]\!]$ return the leaf stomatal conductance (m s^{-1}) at a specific PAR and VPD value, respectively. PAR_{max} is the maximum PAR (W m^{-2}) at which oil palm leaf stomatal conductance no longer increases with PAR. Its value was set at 330 W m^{-2} (or 1500 μmol m^{-2} s^{-1}) [86]. VPD_{min} is the minimum vapor pressure deficit (mbar), which was assigned as 10 mbar for oil palm [86,87]. VPD is the difference between the saturated vapor pressure and air vapor pressure. At VPD_{min}, leaf stomatal conductance is maximum and will decline with rising VPD.

2.5. Soil water component

2.5.1. Water fluxes

The entire soil profile, extending from the surface to the root zone, was partitioned into a minimum of three consecutive layers. Water movement within each soil stratum was modeled using the "tipping bucket" method, where water flows from the topmost layer and subsequently flowing into the layers beneath [88]. The water balance calculations presumed the absence of surface runoff or groundwater. Furthermore, it was assumed that the soil below the last layer in the profile maintained a constant moisture content equivalent to that of the final layer [88]. Consequently, the water flow exiting the last soil layer was attributed solely to gravitational forces.

Darcy's law was used to describe the one-dimensional water flow from one soil layer to another (Eq. 26a-b). Water flux into soil layer no. I is q_i (m day^{-1}), which was determined by

$$q_i = \begin{cases} MIN\left[K_{s,1}, P_{net}\right] - ET_s - ET_{c,i} & i = 1 \\ \overline{K}_{\theta,i}\dfrac{(H_{T,i} - H_{T,i-1})}{(z_i - z_{i-1})} - ET_{c,i} & 1 < i \le N \\ K_{\theta,N} & i = N+1 \end{cases} \tag{26a}$$

$$\overline{K}_{\theta,i} = \left[K_{\theta,i-1} - K_{\theta,i}\right] / \left[ln\left(K_{\theta,i-1}\right) - ln\left(K_{\theta,i}\right)\right] \tag{26b}$$

where the subscript i represents soil layer i ($i = 1$ to N, with N being the total number of layers) and i-1 as the layer above I; P_{net} is the net daily rainfall (m day^{-1}); H_T is the total head (m); ET_s and ET_c are the actual evaporation and actual transpiration, respectively (m day^{-1}); and $\overline{K}$ is the logarithmic mean of hydraulic conductivities for layers i and i-1 (m day^{-1}), as per Bittelli et al. [89]. In the first layer, water entry was limited by P_{net} or $K_{s,1}$. The water flux exiting the last layer ($i = N$), q_{N+1} equaled $K_{\theta,N}$ due to the assumption that the underlying soil was uniformly wet with the same water content as the previous layer.

The saturated K_s and unsaturated K_θ soil hydraulic conductivity (all in m day^{-1}) were determined from Bittelli et al. [89], and soil matric suction H_m (m) from Saxton and Rawls [90], so that the total hydraulic gradient H_T (m) is the sum of matric suction and gravity heads, where the latter is equal to the depth of a given soil layer from the soil surface.

The water extracted by the roots in each soil layer i for $ET_{c,i}$ was derived from the plant water uptake algorithm by Miyazaki [91], following a 4:3:2:1 soil water extraction ratio. Based on field measurements by Nelson et al. [92], oil palm roots generally followed this extraction ratio: starting at the soil surface, they extracted about 40 %, 30 %, 20 %, and 10 % of water from each successive quarter segment of the root zone depth.

The net rainfall P_{net} (m) is the amount of rain reaching the ground below the canopies as throughfall and stemflow. The ratio between net rainfall P_{net} and gross rainfall P_{gross} (Eq. (27)) under oil palm canopies for various tree ages was determined by Farmanta [93] as follows:

$$P_{net} / P_{gross} = MAX(0.7295, 1 - 0.0541L) \tag{27}$$

where the MAX function ensures that the net rainfall under full canopies never exceeds the mean of 72.95 % of the gross rainfall, as per observations.

Finally, the net daily change in soil water content in soil layer i is equal to the net flux of the layer, which is determined as the difference between the influx and outflux.

2.5.2. Actual evapotranspiration

Actual evaporation ET_s (m day^{-1}) occurs only from the first soil layer, and was determined by reducing the potential soil evaporation PET_s (m day^{-1}) by a reduction factor $R_{D,e}$ (0–1), following van Keulen and Seligman [94], described by Eq. 28a-b as follows:

$$ET_s = PET_s \cdot R_{D,e} \tag{28a}$$

$$R_{D,e} = \left[1 + \left(3.6073\theta_1/\theta_{s,1}\right)^{-9.3172}\right]^{-1} \tag{28b}$$

Similarly, actual transpiration ET_c (m day^{-1}) was determined by reducing the potential transpiration PET_c (m day^{-1}) by a reduction factor $R_{D,c}$ (equivalent to f_{water} in Eq. (23)), following Kropff [85], or

$$ET_c = PET_c \cdot R_{D,c} \tag{29a}$$

$$R_{D,c} = f_{water} = \begin{cases} 1 & \theta_{root} \geq \theta_{cr,root} \\ \dfrac{\theta_{root} - \theta_{1500,root}}{\theta_{cr,root} - \theta_{1500,root}} & \theta_{1500,root} < \theta_{root} < \theta_{cr,root} \\ 0 & \theta_{root} \leq \theta_{1500,root} \end{cases} \tag{29b}$$

$$\theta_{cr,root} = \theta_{1500,root} + p\left(\theta_{33,root} - \theta_{1500,root}\right) \tag{29c}$$

where θ_{root} is the volumetric water content in the root zone (m^3 m^{-3}); subscripts 33 and 1500 denote the field capacity and permanent wilting point, respectively (m^3 m^{-3}); and $\theta_{cr,root}$ is the critical volumetric water content in the root zone, below which water stress occurs (m^3 m^{-3}). Soil water measurements by Foong [95] in irrigated and non-irrigated oil palm trials suggested that the critical soil water content below which oil palm suffers from water stress was approximately 50 % of the available water content (AWC). Similarly, Rey et al. [96] also observed that oil palm stomatal conductance declined when the soil water content fell below a level between 40 and 50 % of AWC. Hence, p in Eq. (29c) was taken as 0.5. The amount of water in the root zone θ_{root} is simply the summation of the water content from the first soil layer ($i = 1$) until the rooting depth.

The volumetric soil water content at saturation, field capacity, and permanent wilting point were estimated based on the soil's clay and sand contents, following Saxton et al. [97], as their estimates were found to be slightly more accurate by Teh and Iba [98] for Malaysian mineral soils than the more recent work by Saxton and Rawls [90].

2.6. Crop growth component

2.6.1. Maintenance respiration

Gross assimilates produced via photosynthesis are first channeled for plant maintenance (supporting processes for continual plant survival) and then for growth (synthesis of new cells). The method by van Kraalingen et al. [43] for oil palm was adapted. The maintenance respiration of the leaves, trunk, roots, inflorescences, and bunches in this study was estimated based on their biomass dry weights and their protein and mineral content. For inflorescences and bunches, where their protein and mineral content measurements were unavailable, their estimates could be derived using the protein and mineral content of the rachis [8,43]. As stated earlier,

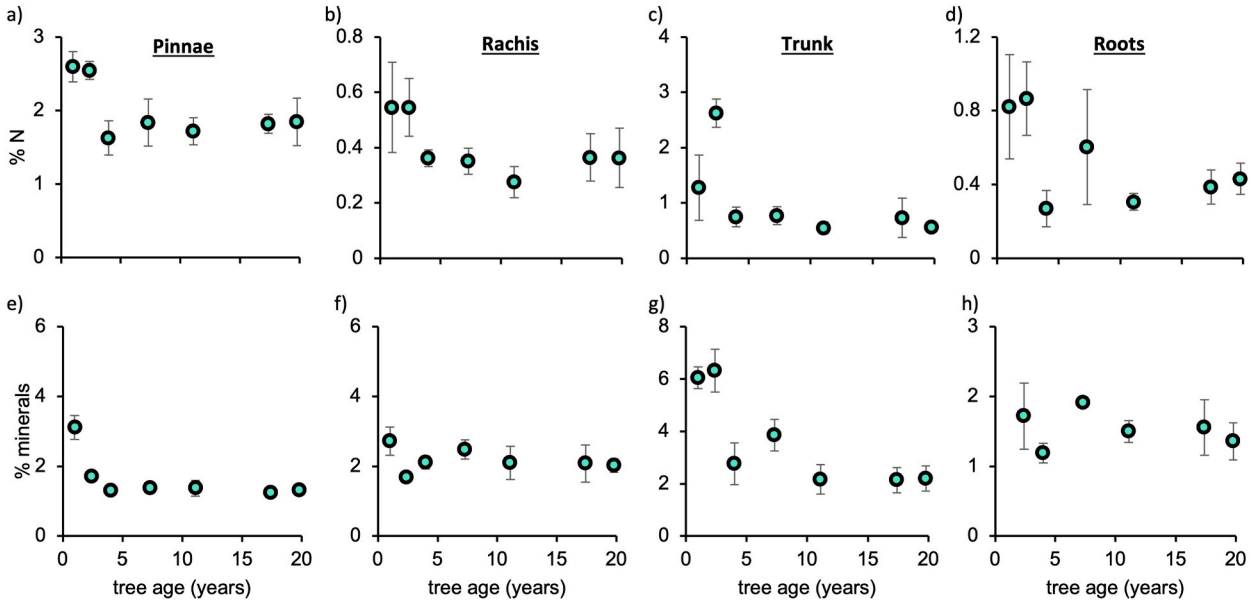

Fig. 6. Changes in the distribution of nitrogen (N) (a–d) and other mineral nutrients (e–h) across different parts of the oil palm tenera tree with increasing age [51]. Mean (±1 SD) values (N = 4 per age group) are shown for the pinnae (a, e), rachis (b, f), trunk (c, g), and roots (d, h).

maintenance calculations require information about protein content. As we did not measure protein content, the N content was measured and converted into protein using a conversion factor of 6.25, since every 6.25 g of protein comprised 1 g of N [99]. The mineral content was taken as the sum of the major nutrients P, K, Mg, and Ca. Micronutrients were not included as they were not measured in the various tree parts, and compared with macronutrients, their total content in plants is smaller by at least one order of magnitude [100].

Based on the dry matter and nutrient partitioning data obtained by Ng et al. [41], van Kraalingen et al. [43] estimated the maintenance respiration of each tree part. However, Ng et al. [41] sampled trees from older dura planting material, which has long been replaced by thin-shelled tenera as the main commercial planting material because of its greater oil yield potential (9.5 t oil ha^{-1}) [42,101]. Recognizing this, Cheah et al. [51] updated the work by Ng et al. [41] by not only measuring the newer tenera oil palm planting material but also measuring them in greater numbers (Fig. 6). Sawit.jl utilized the data from Cheah et al. [51], which includes the N distribution in the pinnae, rachis, trunk, and roots (Fig. 6a–d) and the distribution of other mineral nutrients in the same tree parts (Fig. 6e–h), to calculate the maintenance respiration of various tree parts following the methodology of van Kraalingen et al. [43].

2.6.2. Growth respiration

Assimilates in excess after maintenance respiration would then be channeled for growth respiration G_{gro} (kg DM $palm^{-1}$ day^{-1}). Following van Kraalingen et al. [43], the growth respiration rate for a specific tree part $G_{(part)}$ was calculated by multiplying the proportion of that part relative to all the vegetative tree parts by G_{gro}; thus, the dry weight of the tree part at time t_1 could be incremented for the subsequent time t_2 using Euler's integration method (Eq. (30)):

$$W_{(part),t2} = W_{(part),t1} + G_{(part)} - G_{death,(part)} \tag{30}$$

where $W_{(part)}$ is the dry weight of a tree part (pinnae, rachis, trunk, or roots) (kg DM $palm^{-1}$); and $G_{(part)}$ and $G_{death,(part)}$ are the growth and death rates of a tree part, respectively. Leaf (pinnae and rachis) deaths are caused by aging, and they were determined by Eq. 31a-b as follows:

$$G_{death,(pinnae\ and\ rachis)} = \begin{cases} 0 & age \le 600 \\ f\left(\dfrac{age - 600}{2400 - 600}\right) & 600 < age \le 2400 \\ f & age > 2400 \end{cases} \tag{31a}$$

where *age* is the tree age (days); and f is the leaf death rate, and its value can be amplified by water stress $R_{D,c}$ (Eq. (29a)) as

$$f = 0.0013\left[1 + (0.6 - 0.01S)\left(1 - R_{D,c}\right)\right]; \quad 0 \le f \le 0.0013 \tag{31b}$$

where S is the sand content in the root zone (%). The death rate of roots $G_{death,(roots)}$ (kg DM $palm^{-1}$ day^{-1}) was determined by:

$$G_{death,(roots)} = \begin{cases} 0 & age \le 1200 \\ 0.2/365 & age > 1200 \end{cases} \tag{32}$$

The values for these death rates (Eqs. (31) and (32)) were obtained from Dr. Ian E. Henson, then at the Malaysian Palm Oil Board (personal communication). It was assumed that the trunk experienced no death; thus, $G_{death,(trunk)}$ equaled zero [43].

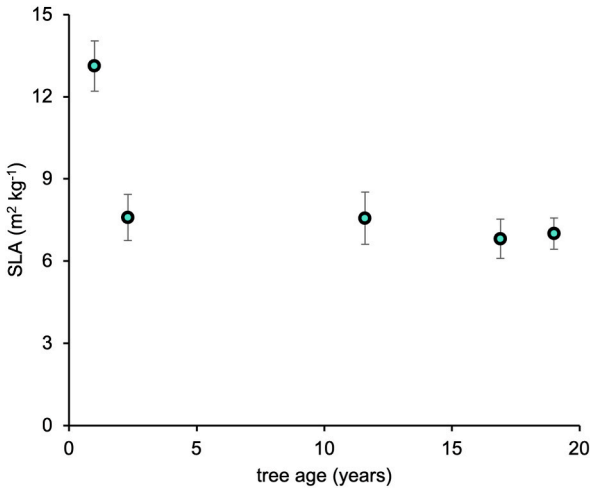

Fig. 7. Mean (±1 SD) changes in specific leaf area (SLA) of oil palm with tree age [51].

The increase in leaf area index L (m^2 leaf m^{-2} ground) was determined by multiplying the pinnae dry weight by the specific leaf area SLA (m^2 leaf kg^{-1} DM). For oil palm, the change in SLA with increasing tree age from 1 to 19 years was measured by Cheah et al. [51] (Fig. 7).

We observed that the growth rate of trunk height increased linearly from year 1 until year 11, after which the growth rate of the trunk was constant at Δh_{max}. Using measured trunk height data of oil palm grown in various soil textures from Refs. [102–107], Δh_{max} (m yr^{-1}) was related to the planting density and sand content in the root zone according to Eq. (33):

$$\Delta h_{max} = a + bPD + cS \tag{33}$$

where the parameters a, b, and c are 0.274425, 0.000307, and 0.002212, respectively. The growth rate of the trunk Δh (m yr^{-1}) was determined using Eq. (34) as follows:

$$\Delta h = \begin{cases} \Delta h_{max}(age/365 - 1)/10 & age/365 < 11 \\ \Delta h_{max} & age/365 \geq 11 \end{cases} \tag{34}$$

so that the trunk height h_{trunk} (m) was determined using Eq. (35) as follows:

$$h_{trunk} = \Delta h \times age/365 \tag{35}$$

Change in oil palm canopy height h_{canopy} (m) was determined by Cheah et al. [51] as follows:

$$h_{canopy} = 1.5091 + 0.001382age \tag{36}$$

Consequently, the full tree height h (m) is simply the sum of h_{trunk} (Eq. (35)) and h_{canopy} (Eq. (36)).

The increase in the rooting depth d_{root} (m) between two successive days t_1 and t_2 was determined using Eq. (37) as follows:

$$d_{root,t2} = d_{root,t1} + \left(d_{g,root} \times R_{D,c}\right) \tag{37}$$

where $d_{g,root}$ is the daily increase in the rooting depth, taken as 0.002 m day^{-1}, the mean value of root growth for oil palm [108,109]. Note that the increase in rooting depth would be adversely affected by water stress $R_{D,c}$ [85].

2.6.3. Generative growth

The amount of assimilates in excess after growth respiration is available for generative growth G_{gen} (kg CH_2O $palm^{-1}$ day^{-1}). These available assimilates would be used for the growth of generative organs, such as male flowers, immature bunches, and mature bunches. The "boxcar train" method by van Kraalingen et al. [43] was adapted to monitor the growth progression of these generative organs [110].

In this method, three trains symbolize the growth of each generative organ (Supplementary Fig. S1a-b). Each train also comprises multiple boxcars; therefore, each boxcar represents an age class. The life expectancy for male flowers and immature bunches was set at 210 days, and for mature bunches at 150 days, with a one-day model time step [111]. In every daily time step, the following algorithm would be applied for each boxcar in each train: 1) the weight in each age class (including zero weight) would be transferred to progressively older age classes, then 2) only the nonzero weight in each age class would be incremented based on the calculated growth rate. The lifespan of the male flowers was 210 days. For immature bunches, the day after 210 days signified the pollination point, followed by the growth of the pollinated bunch (*i.e.*, mature bunches) until the end of the next 150 days, when yield would finally be produced. Calculations to determine the growth rates of the generative organs followed van Kraalingen et al. [43] to ultimately give the total weight for a given generative organ, which is simply the summation of the weights in all boxcars for that generative organ.

van Kraalingen et al. [43] assumed both male and female flowers always occurred in equal proportions and without risk of flower abortion. Here, an algorithm was introduced for flower sex determination (Eq. (38)), whereby the probability of producing female flowers was governed by the current water stress level $R_{D,c}$ (Eq. (29b)) and the genetic predisposition or probability p_{female} to produce female flowers, or

$$sex\ of\ new\ flower = \begin{cases} female & r \leq \left(R_{D,c} \bullet p_{female}\right) \\ male & r > \left(R_{D,c} \bullet p_{female}\right) \end{cases} \tag{38}$$

where p_{female} has the extrema of 0 and 1 for never and always female, respectively; and r is a random variable uniformly distributed on [0 to 1). Chances of female flowers would decrease the lower the female flower predisposition and the higher the water stress level. In addition, flower abortion may occur 9 months before harvest, according to Corley et al. [111], and abortion occurs if the generated random value is larger than $R_{D,c}$. In this study, because the genetic predisposition to form female flowers is unknown, p_{female} was set at 0.5, as used by van Kraalingen et al. [43], to mean a 50-50 chance of producing female flowers.

2.7. Required model parameters

Sawit.jl requires the following parameters: 1) site latitude; 2) site daily weather for the entire simulation period (*i.e.*, minimum and maximum air temperature, wind speed, and rainfall); 3) date of field planting; 4) planting density; 5) soil layer properties (soil texture,

Table 2
Independent datasets from seven sites used to validate the Sawit.jl model. The planting material for all seven sites was Deli dura × AVROS pisifera (tenera).

Sites							
Properties	Kerayong	Merlimau	Rengam	Sabrang	Seri Intan	Sg. Buloh	Kalumpong[a]
Latitude (° N)	3.17	2.25	1.88	3.79	3.97	3.35	4.96
Longitude (° E)	101.34	102.45	103.39	100.97	100.98	101.32	100.57
Planting density (palms ha^{-1})	136, 160, 185	120, 135, 148, 164, 181, 199, 220, 243, 268, 296	82, 90, 100, 111, 123, 136, 166, 184	136, 170	180	77, 85, 94, 103, 114, 125, 136, 138, 152, 167, 184, 203, 223, 246, 271, 299	124, 126, 138, 146, 150, 150, 150, 154, 158, 159
Field planting date	Dec. 1992	Apr. 1987	Oct. 1982	Mar. 1990	Jan. 2007	Dec. 1988	Feb. 1997
End trial	Dec. 2014	Dec. 2006	Dec. 2001	Dec. 2008	Dec. 2019	Dec. 2007	Feb. 2020
No. of years	22	19	20	19	7	19	23
Soil series	Jawa (Sulfic Endoaquepts)	Rengam (Typic Kandiudult)		Briah (Typic Endoaquepts)		Bernam (Typic Endoaquepts)	Briah and Jawa
Annual weather data (mean ± SD)							
Min. and max. Air temperature (°C)	24.1 ± 0.5 32.8 ± 0.4	23.7 ± 0.4 32.2 ± 0.3	23.4 ± 0.2 33.7 ± 0.6	23.4 ± 0.3 32.3 ± 0.3	23.8 ± 0.4 32.2 ± 0.4	24.2 ± 0.6 32.9 ± 0.4	23.2 ± 0.3 32.8 ± 0.5
Wind speed (m s^{-1})	1.5 ± 0.2	1.6 ± 0.2	1.7 ± 0.1	1.2 ± 0.2	1.2 ± 0.1	1.5 ± 0.2	1.3 ± 0.1
Rain (mm)	2761 ± 322	1952 ± 261	2121 ± 307	1824 ± 259	1833 ± 309	2807 ± 348	2003 ± 408
Soil properties (mean ± SE)							
Sand (%)	6.6 ± 0.9	67.3 ± 0.8	61.1 ± 1.0	19.8 ± 0.1	21.0 ± 0.2	16.7 ± 0.4	47.8 ± 1.4
Clay (%)	51.4 ± 0.4	27.4 ± 0.7	32.7 ± 0.9	53.3 ± 0.4	50.6 ± 0.3	58.5 ± 0.6	13.7 ± 1.8
Organic C (%)	3.9 ± 0.6	1.7 ± 0.1	1.6 ± 0.1	1.3 ± 0.1	8.1 ± 0.2	1.9 ± 0.1	*nd*
Total N (%)	0.34 ± 0.21	0.14 ± 0.01	0.17 ± 0.01	0.19 ± 0.02	0.36 ± 0.01	0.21 ± 0.01	*nd*

[a] Kalumpong has three blocks with the same planting density of 150 palms ha^{-1}; *nd* – not determined.

initial volumetric soil water content, and layer thickness); 6) initial weights of the individual tree parts at the time of field planting; 6) initial and maximum possible rooting depth; 8) change in specific leaf area with tree age; 9) change in nitrogen and mineral content and partitioning in the individual tree parts with tree age; and 10) genetic predisposition to produce female flowers. The individual tree parts considered are the pinnae, rachis, trunk, roots, inflorescence (male and female), and bunches. Values for the first five parameters must be provided by the user. However, for the last five model parameters, the model will use their respective default values if they are not explicitly provided.

2.8. Model validation

Simulations from Sawit.jl were validated against historical data of measured oil palm parameters of growth and yield from seven commercial oil palm plantations owned by Sime Darby Plantation Berhad, around Peninsular Malaysia (Table 2). These sites had

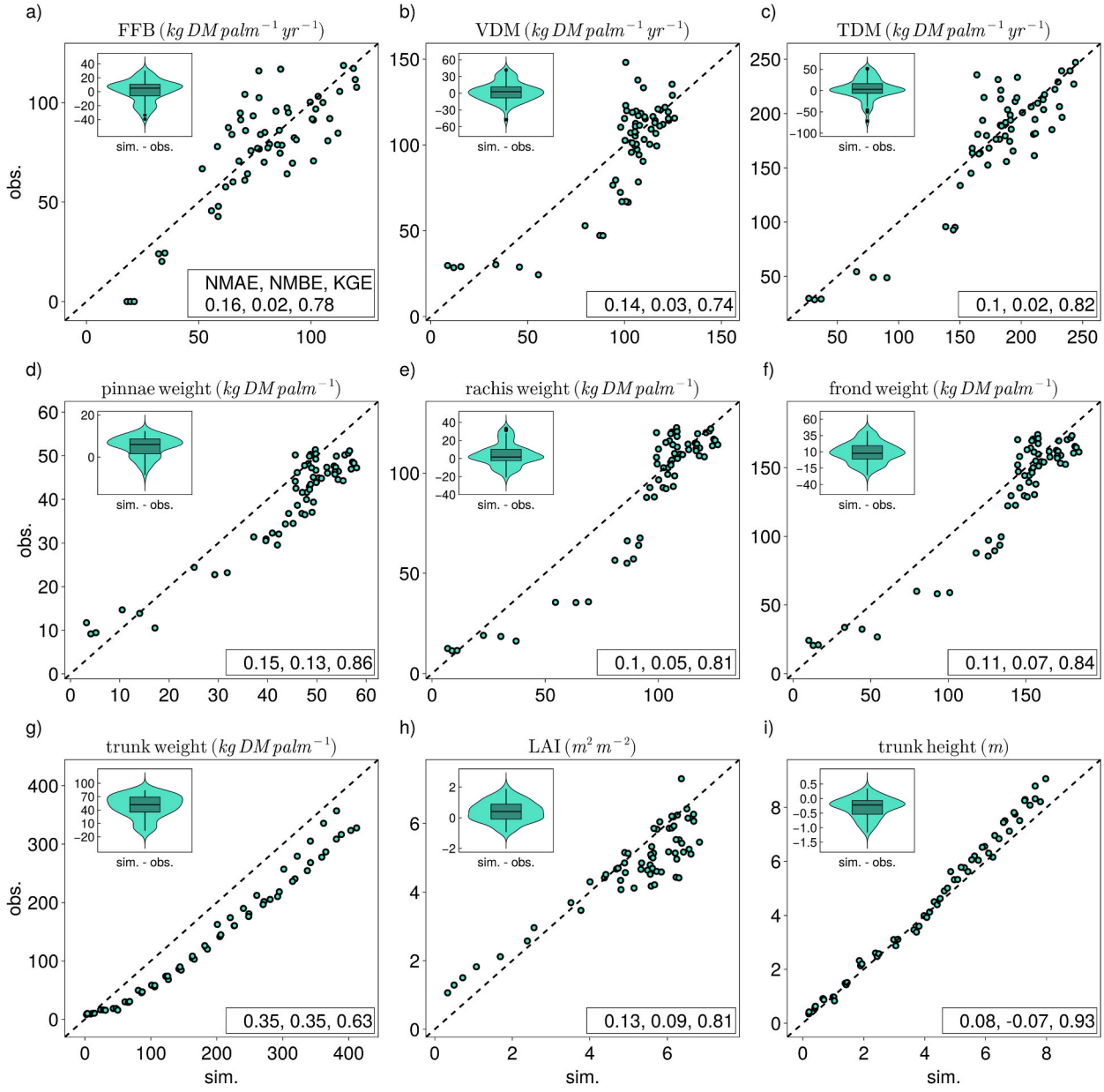

Fig. 8. Kerayong: Agreement between observed (obs.) and simulated (sim.) values across all planting densities for fresh fruit bunches (FFB) yield (a), vegetative dry matter (VDM) (b), total DM (TDM) (c), pinnae weight (d), rachis weight (e), frond weight (f), trunk weight (g), leaf area index (LAI) (h), and trunk height (i). The inset box and violin plots show the distribution of model errors. NMAE, NMBE, and KGE are goodness-of-fit indices.

diverse planting densities, tree ages, soil textures, and rainfall levels. At all sites, oil palm seedlings were transferred from the nursery to be planted in the field at the age of 1 year, following conventional practices. Note that the datasets from seven of these sites were independent and not part of the other datasets used for parameterizing the Sawit.jl model.

Merlimau and Rengam represent a typical Malaysian inland environment, where the Ultisol was developed from granite dominants. Sg. Buloh, Kerayong, Sabrang, and Seri Intan represent a typical Malaysian coastal environment, where Inceptisol was developed from marine alluvium dominants. Kalumpong comprises diverse soil types, with the Briah and Jawa series being predominant.

For all sites, except Seri Intan and Kalumpong, the following oil palm parameters were measured: fresh fruit bunch (FFB) yield, vegetative growth matter production (VDM), total dry matter production (TDM), pinnae dry weight, rachis dry weight, fronds dry weight, trunk dry weight, trunk height, and leaf area index. The following were measured at Seri Intan: FFB yield, leaf area index, and trunk height. At Kalumpong, only the FFB yield was measured.

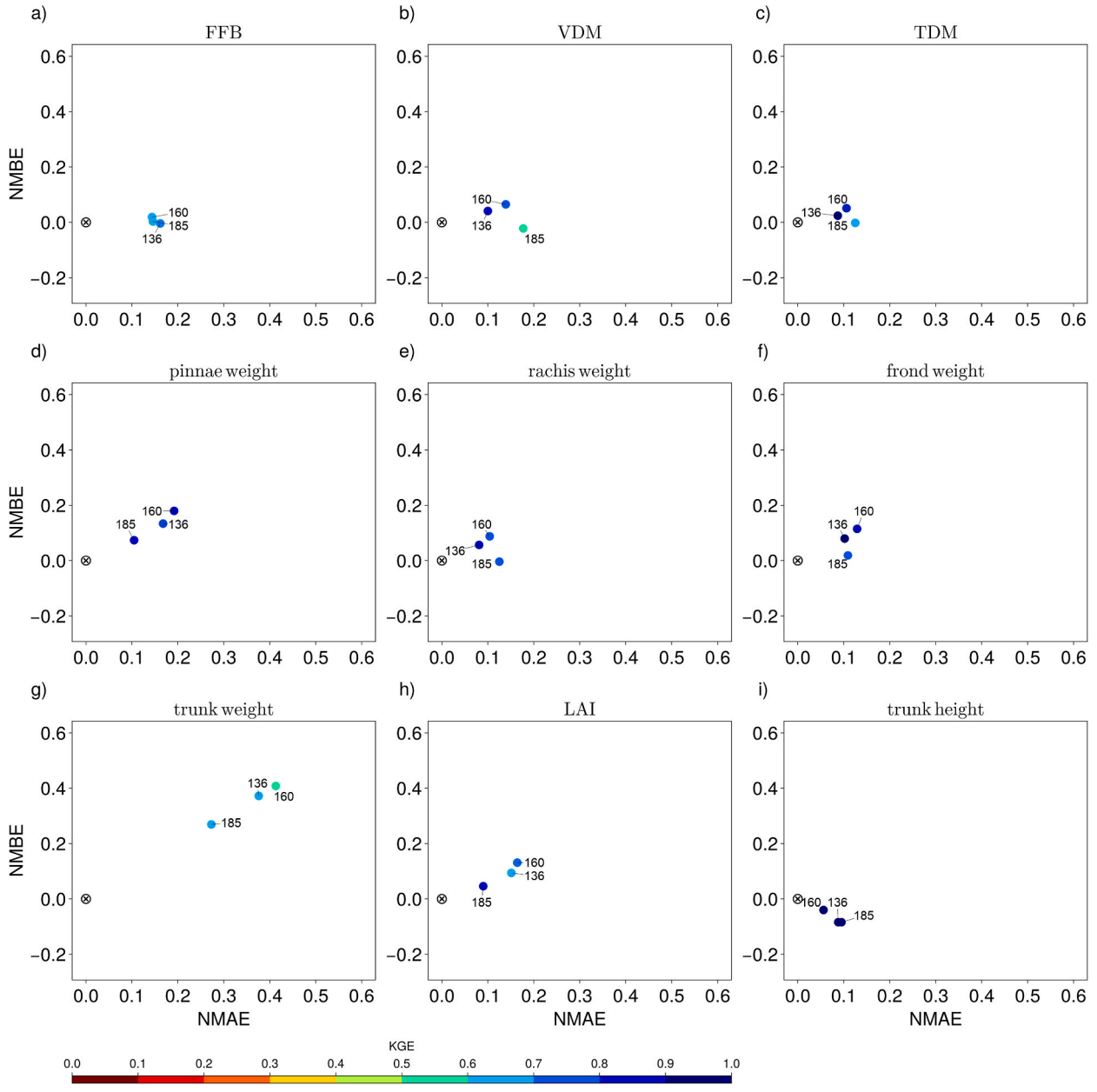

Fig. 9. Kerayong: NMAE, NMBE, and KGE scores for each planting density (numeric labels on markers) for fresh fruit bunches (FFB) yield (a), vegetative dry matter (VDM) (b), total DM (TDM) (c), pinnae weight (d), rachis weight (e), frond weight (f), trunk weight (g), leaf area index (LAI) (h), and trunk height (i). Perfect simulations would have markers in the darkest blue (KGE = 1) and located at ⊗ position for NMAE = 0 and NMBE = 0.

Vegetative growth parameters such as VDM, dry weights of tree parts, trunk height, and leaf area index were calculated annually using nondestructive methods [42,112–114]. FFB yields were measured at 10–12 days interval and summed to give the annual totals. The annual VDM and fruit bunch yields were then summed to obtain the annual TDM.

Sawit.jl requires inputs such as site latitude, daily weather (minimum and maximum air temperatures, wind speed, and rainfall), partitioning of N and mineral contents, SLA, initial soil water content, soil texture, and the initial dry weights of the pinnae, rachis, trunk, and roots. Cheah et al. [51] measured the mean (±SE) initial dry weights in kg DM palm^{-1} for the pinnae, rachis, trunk, and roots as 0.40 ± 0.07, 0.70 ± 0.11, 0.10 ± 0.01, and 0.20 ± 0.03, respectively.

The agreement between the model simulations and observations (measurements) was evaluated by visually examining the agreement plots of the simulated versus observed values and by using goodness-of-fit indices. Three such indices were selected, two of which were normalized mean absolute error (NMAE) and normalized mean bias error (NMBE). NMAE was selected because it denotes the average absolute difference between simulations and observations. It ranges between 0 and $+\infty$, where NMAE = 0 indicates a

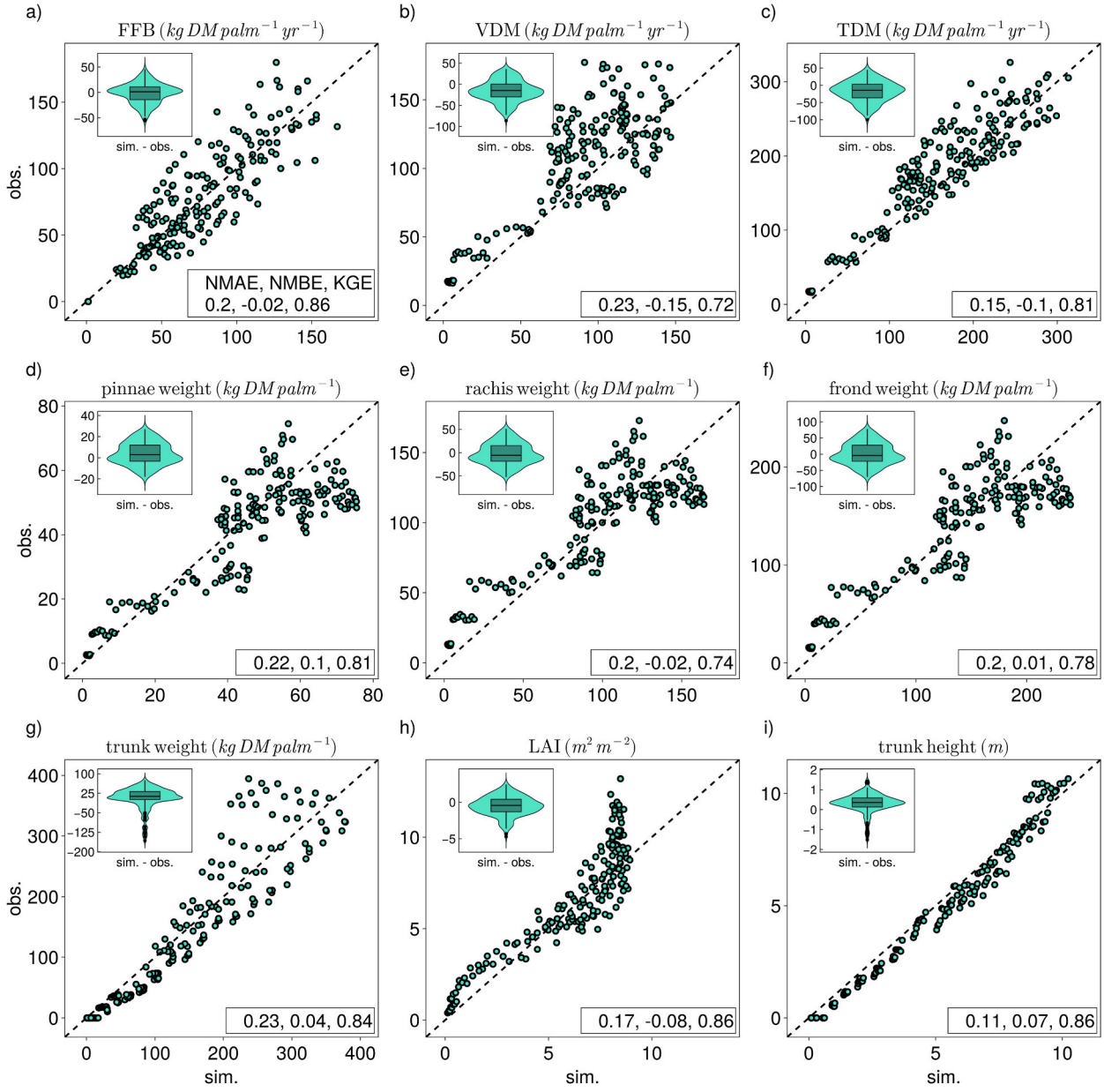

Fig. 10. Merlimau: Agreement between observed (obs.) and simulated (sim.) values across all planting densities for fresh fruit bunches (FFB) yield (a), vegetative dry matter (VDM) (b), total DM (TDM) (c), pinnae weight (d), rachis weight (e), frond weight (f), trunk weight (g), leaf area index (LAI) (h), and trunk height (i). The inset box and violin plots show the distribution of model errors. NMAE, NMBE, and KGE are goodness-of-fit indices.

perfect model. NMBE was also selected because this index indicates the average model bias, that is, the overall tendency of the model to under- (negative bias with negative NMBE values) or overestimate (positive bias with positive NMBE values). It ranges between -∞ and +∞, where NMBE = 0 indicates no overall model bias. NMAE and NME were calculated using Eqs. (39) and (40), respectively, as follows:

$$NMAE = \sum |P_i - O_i| \Big/ \sum O_i \tag{39}$$

$$NMBE = \sum (P_i - O_i) \Big/ \sum O_i \tag{40}$$

where P_i and O_i are the predicted (simulated) and observed (measured) values, respectively. NMAE and NMBE are normalized to

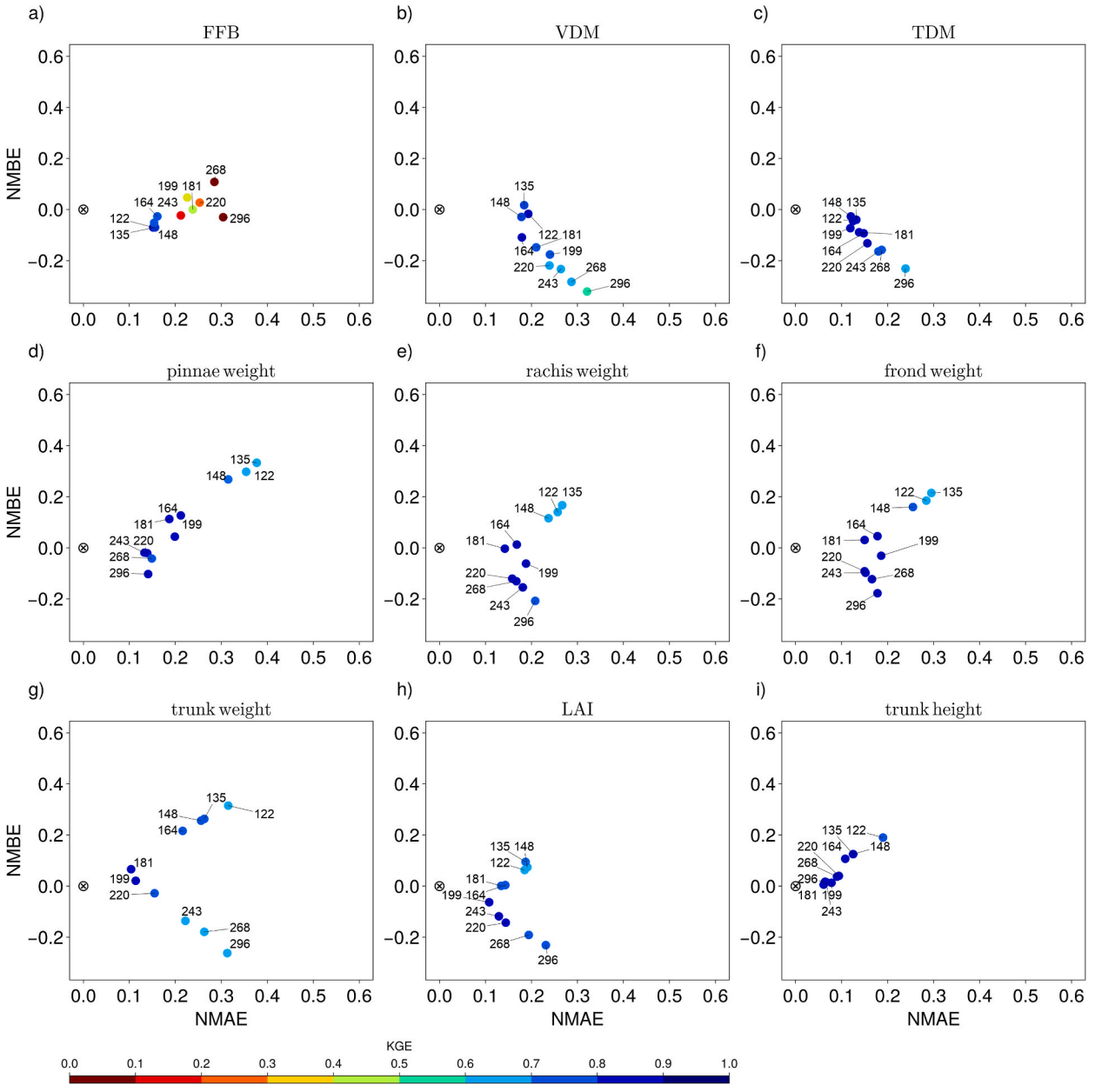

Fig. 11. Merlimau: NMAE, NMBE, and KGE scores for each planting density (numeric labels on markers) for fresh fruit bunches (FFB) yield (a), vegetative dry matter (VDM) (b), total DM (TDM) (c), pinnae weight (d), rachis weight (e), frond weight (f), trunk weight (g), leaf area index (LAI) (h), and trunk height (i). Perfect simulations would have markers in the darkest blue (KGE = 1) and located at ⊗ position for NMAE = 0 and NMBE = 0.

remove dependence on the scale of the datasets being compared. These indices can be converted to percentages by multiplying them by 100 %. For example, an NMAE of 0.05 is equivalent to an average absolute error of 5 % of the observations, and an NMBE of +0.1 is an average overestimation of 10 % of the observations.

The third selected index was the Kling-Gupta Efficiency (KGE) [115]. The KGE creates a single score out of three model agreement properties (Eq. (41)): linear correlation coefficient r, mean μ, and coefficient of variation cv between simulations and observations as

$$KGE = 1 - \sqrt{(r-1)^2 + \left(\mu_p / \mu_o - 1\right)^2 + \left(cv_p / cv_o - 1\right)^2} \tag{41}$$

where subscripts p and o denote the predicted and observed values, respectively. KGE is a useful metric because it is less sensitive to outliers [116], and it simultaneously evaluates three conditions, such that a perfect model has a perfect linear correlation, equal mean,

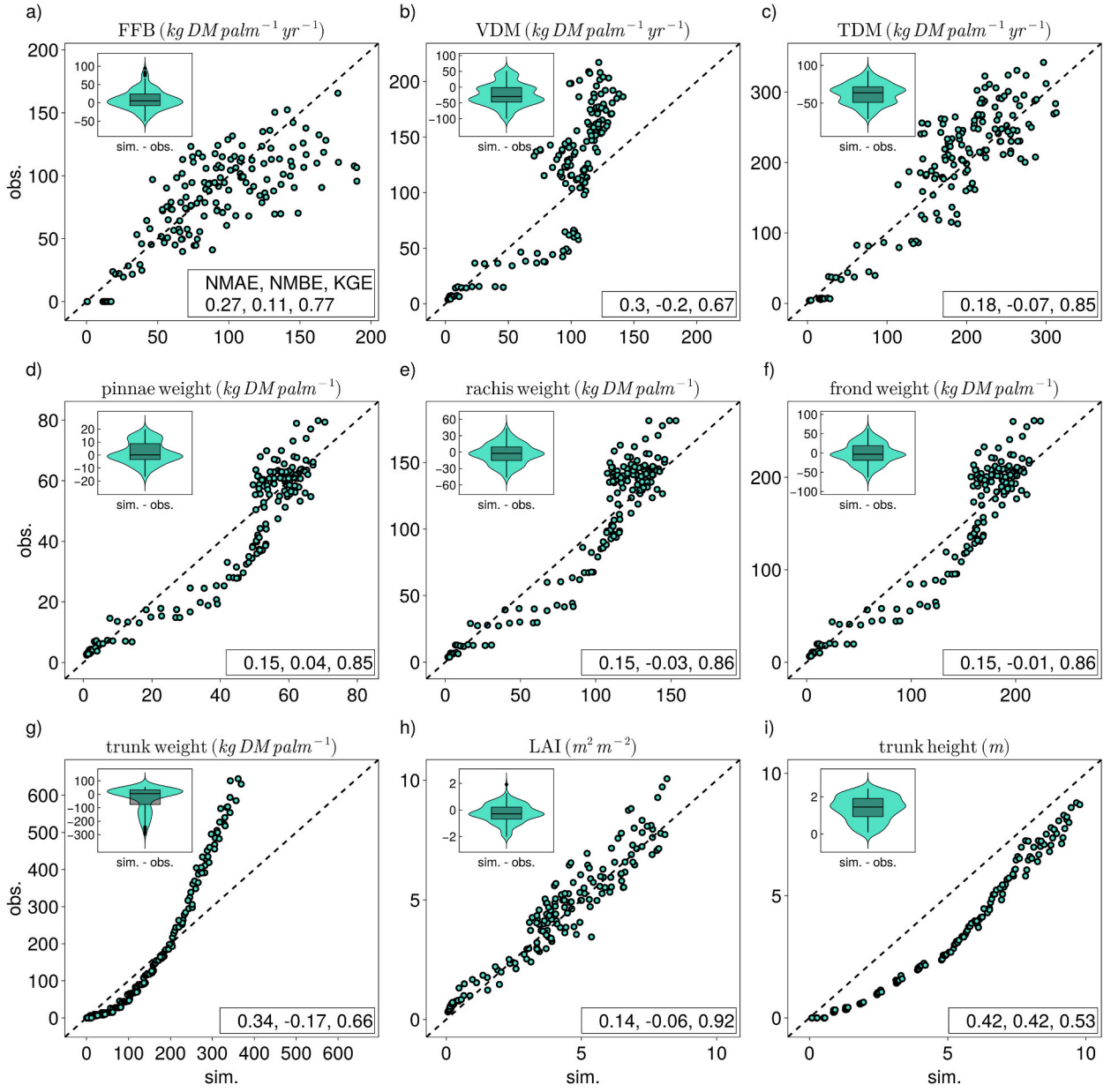

Fig. 12. Rengam: Agreement between observed (obs.) and simulated (sim.) values across all planting densities for fresh fruit bunches (FFB) yield (a), vegetative dry matter (VDM) (b), total DM (TDM) (c), pinnae weight (d), rachis weight (e), frond weight (f), trunk weight (g), leaf area index (LAI) (h), and trunk height (i). The inset box and violin plots show the distribution of model errors. NMAE, NMBE, and KGE are goodness-of-fit indices.

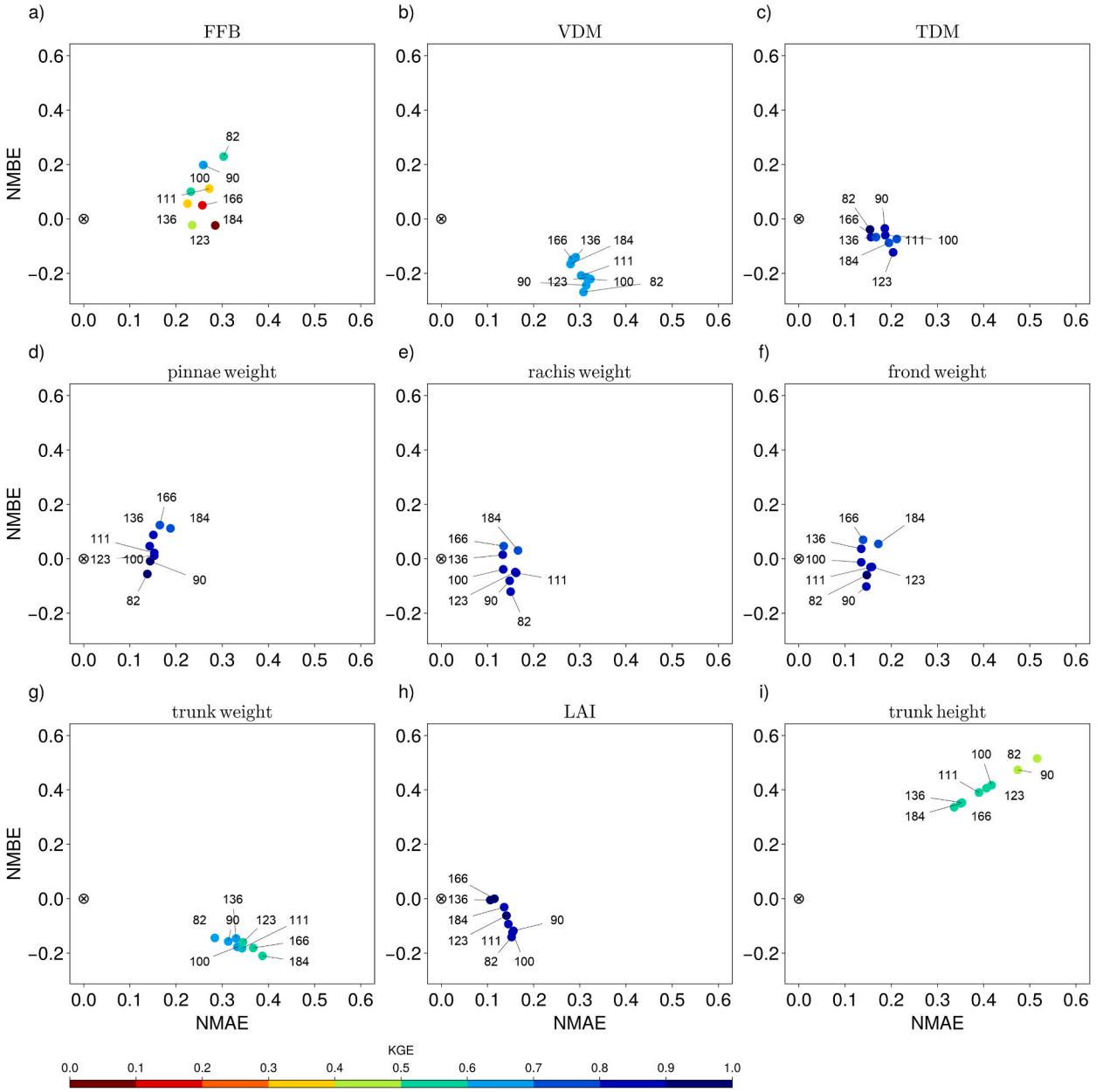

Fig. 13. Rengam: NMAE, NMBE, and KGE scores for each planting density (numeric labels on markers) for fresh fruit bunches (FFB) yield (a), vegetative dry matter (VDM) (b), total DM (TDM) (c), pinnae weight (d), rachis weight (e), frond weight (f), trunk weight (g), leaf area index (LAI) (h), and trunk height (i). Perfect simulations would have markers in the darkest blue (KGE = 1) and located at ⊗ position for NMAE = 0 and NMBE = 0.

and equal coefficient of variation with observations (*i.e.*, $r = 1$, $\mu_p = \mu_o$, and $cv_p = cv_o$). Deviations from these criteria will reduce the KGE score. KGE ranges between -∞ and +1, with +1 denoting a perfect model. According to Knoben et al. [116], model accuracy increasingly improves the higher the KGE score is above −0.41, because at this threshold, the model produces only constant estimates with values equal to mean observations, but they have no correlation with observations and have zero variance due to their constancy. This means $r = 0$, $\mu_p = \mu_o$, and $cv_p = 0$ in Eq. (41) to give KGE $= 1 - \sqrt{2} = -0.41$.

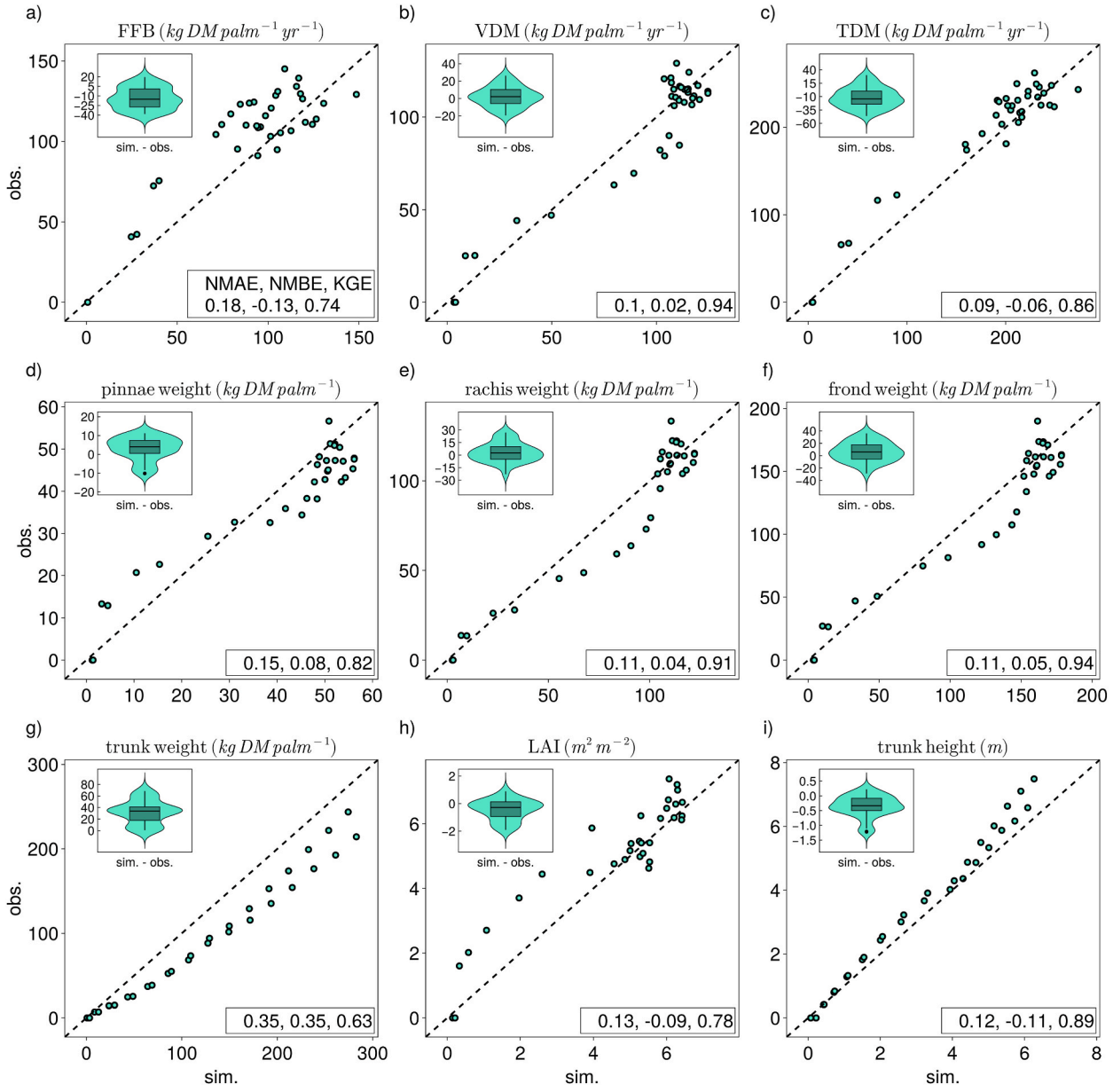

Fig. 14. Sabrang: Agreement between observed (obs.) and simulated (sim.) values across all planting densities for fresh fruit bunches (FFB) yield (a), vegetative dry matter (VDM) (b), total DM (TDM) (c), pinnae weight (d), rachis weight (e), frond weight (f), trunk weight (g), leaf area index (LAI) (h), and trunk height (i). The inset box and violin plots show the distribution of model errors. NMAE, NMBE, and KGE are goodness-of-fit indices.

3. Results

3.1. Model agreement

Individual agreement plots between the observations and simulations for each oil palm parameter, planting density, and site are shown in Supplementary Fig. S2a-r to S4a-r (Kerayong site), S5a-r to S13a-r (Merlimau), S14a-r to S19a-r (Rengam), S20a-r to S22a-r (Sabrang), and S23a-r to S33a-r (Sg. Buloh). For Kalumpong, only yield was measured, and the corresponding agreement plots by planting density are presented in Supplementary Fig. S34a-t. This section presents: 1) the agreement plots that compare observations and simulations for each site across all planting densities, and 2) the goodness-of-fit index scores for every planting density at each site (Figs. 8a-i to 17a-i, 18a-f, and 19a-b).

The agreement between observations and model simulations was generally good, although the model accuracy depended on the oil

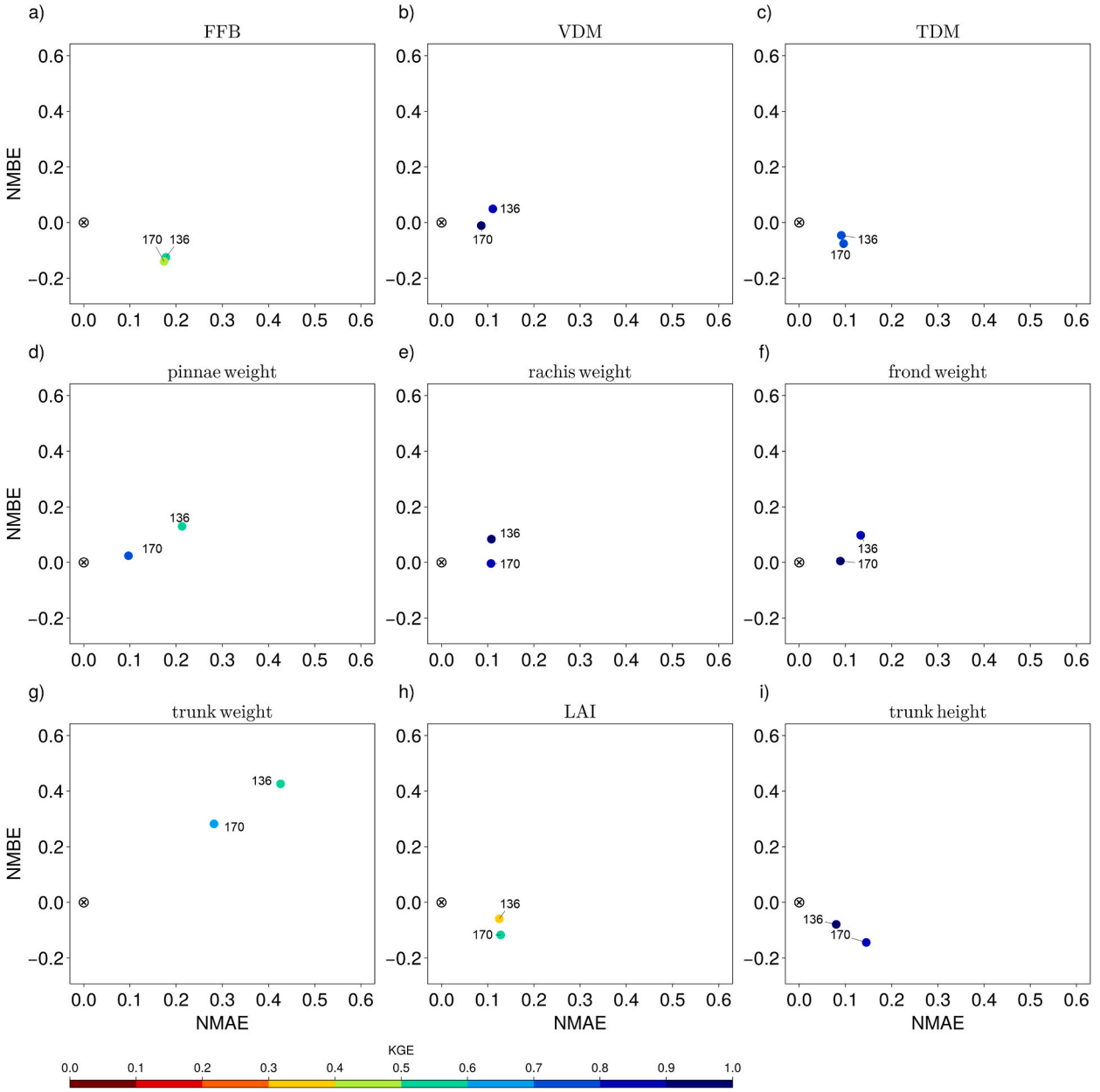

Fig. 15. Sabrang: NMAE, NMBE, and KGE scores for each planting density (numeric labels on markers) for fresh fruit bunches (FFB) yield (a), vegetative dry matter (VDM) (b), total DM (TDM) (c), pinnae weight (d), rachis weight (e), frond weight (f), trunk weight (g), leaf area index (LAI) (h), and trunk height (i). Perfect simulations would have markers in the darkest blue (KGE = 1) and located at ⊗ position for NMAE = 0 and NMBE = 0.

palm parameter being simulated, site, and planting density. Fresh fruit bunch (FFB) yield is often the most important oil palm parameter. Yield simulations were generally accurate for Kerayong (Figs. 8a and 9a), Seri Intan (Fig. 18a and d), and Kalumpong (Fig. 19a and b), with a small Normalized Mean Bias Error (NMBE) between −2 and 6 %, relatively low Normalized Mean Absolute Error (NMAE) below 16 %, and moderate to strong positive Kling-Gupta Efficiency (KGE) scores between 0.6 and 0.9. For Merlimau, model simulations clustered along the 1:1 line of agreement (Fig. 10a), but upon closer inspection, model errors increased with higher planting density (Fig. 11a), whereas the reverse was true for Rengam (Fig. 12a and 13a). Yield simulations for Sabrang were mostly accurate, with a strong KGE of 0.74, but the model underestimated the yield (NMBE = −13 %) for only two planting densities at this site (Fig. 14a and 15a). For Sg. Buloh, FFB yield simulations matched observations well (Fig. 16a), although the accuracy was relatively low for the two highest planting densities (271 and 299 palms ha^{-1}) (Fig. 17a).

Because total dry matter (TDM) production includes vegetative dry matter (VDM) production, the model agreement for TDM

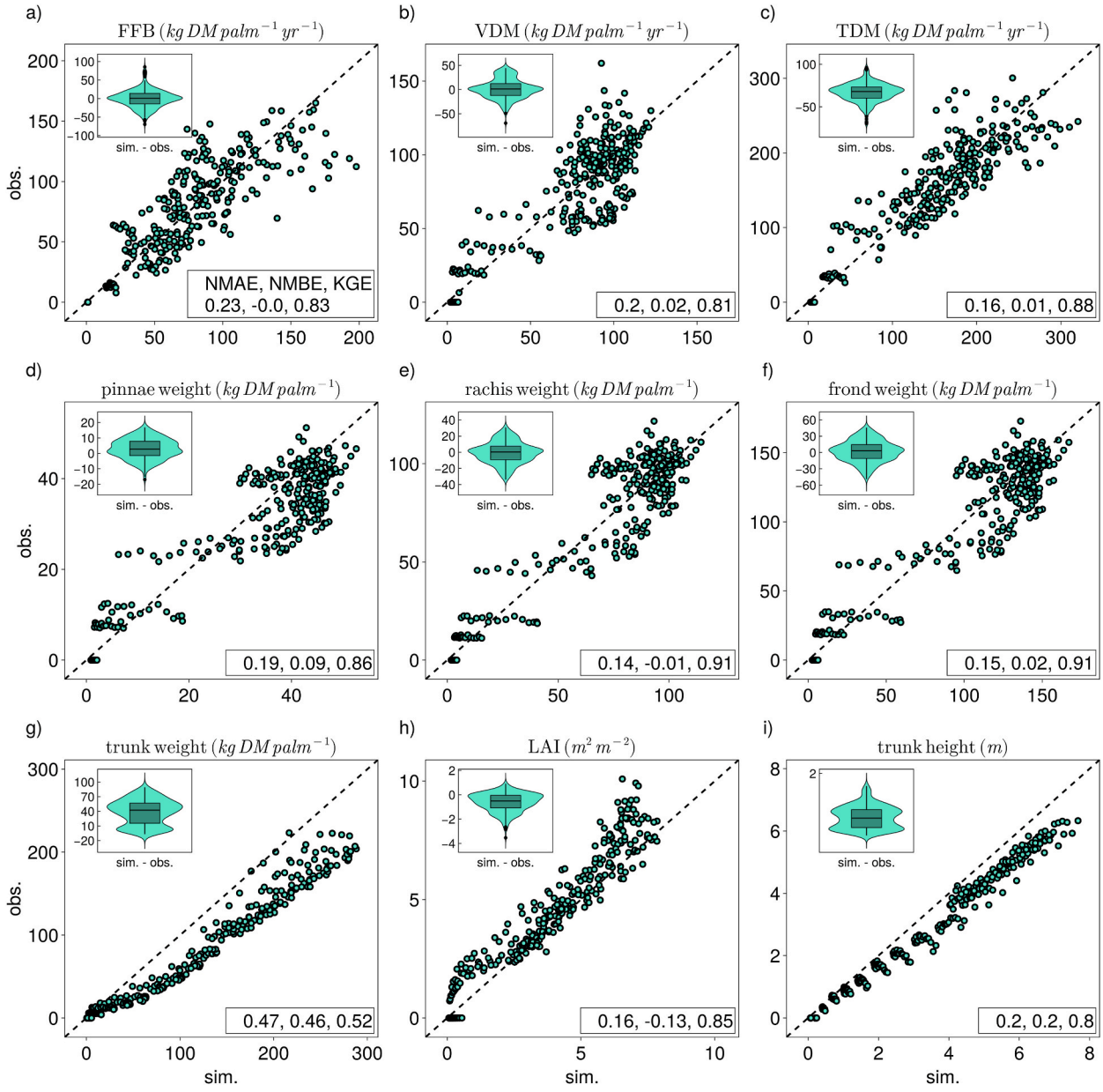

Fig. 16. Sg. Buloh: Agreement between observed (obs.) and simulated (sim.) values across all planting densities for fresh fruit bunches (FFB) yield (a), vegetative dry matter (VDM) (b), total DM (TDM) (c), pinnae weight (d), rachis weight (e), frond weight (f), trunk weight (g), leaf area index (LAI) (h), and trunk height (i). The inset box and violin plots show the distribution of model errors. NMAE, NMBE, and KGE are goodness-of-fit indices.

generally followed a trend similar to that of VDM. Both VDM and TDM simulations for Kerayong (Fig. 8b and c and 9b-c), Sabrang (Figs. 14b and c and 15b-c), and Sg. Buloh (Figs. 16b and c and 17b-c) had small biases (NMBE between −6 and 3 %), low absolute errors (NMAE <20 %), and strong positive KGE scores ≥0.74. For Merlimau, model errors increased with planting density (Figs. 10b and c and 11b-c), whereas for Rengam, the absolute errors were rather high at 18 and 30 % for VDM and TDM, respectively, for all planting densities (Figs. 12b and c and 13b-c). VDM and TDM were not measured at other sites.

The model accuracy for the leaf dry weights of the pinnae, rachis, and fronds varied depending on the site. The simulations for Kerayong generally showed good agreement with the observations, with an overestimation of ≤15 % (Figs. 8d-f and 9d-f). Simulations for Rengam were accurate overall, with a small NMBE between −1% and 4 %, relatively low NMAE at 15 %, and strong positive KGE scores ≥0.85 (Figs. 12d-f and 13d-f). However, the model overestimated leaf dry weights at mid-range values (Fig. 12d). For Sabrang, the model exhibited a small bias (Figs. 14d-f and 15d-f), whereas for Sg. Buloh, simulations of rachis and frond dry weights agreed closer to observations than pinnae dry weights, with a high KGE ≥0.86 and low NMAE ≤19 % (Fig. 16d-f and 17d-f). However, the two

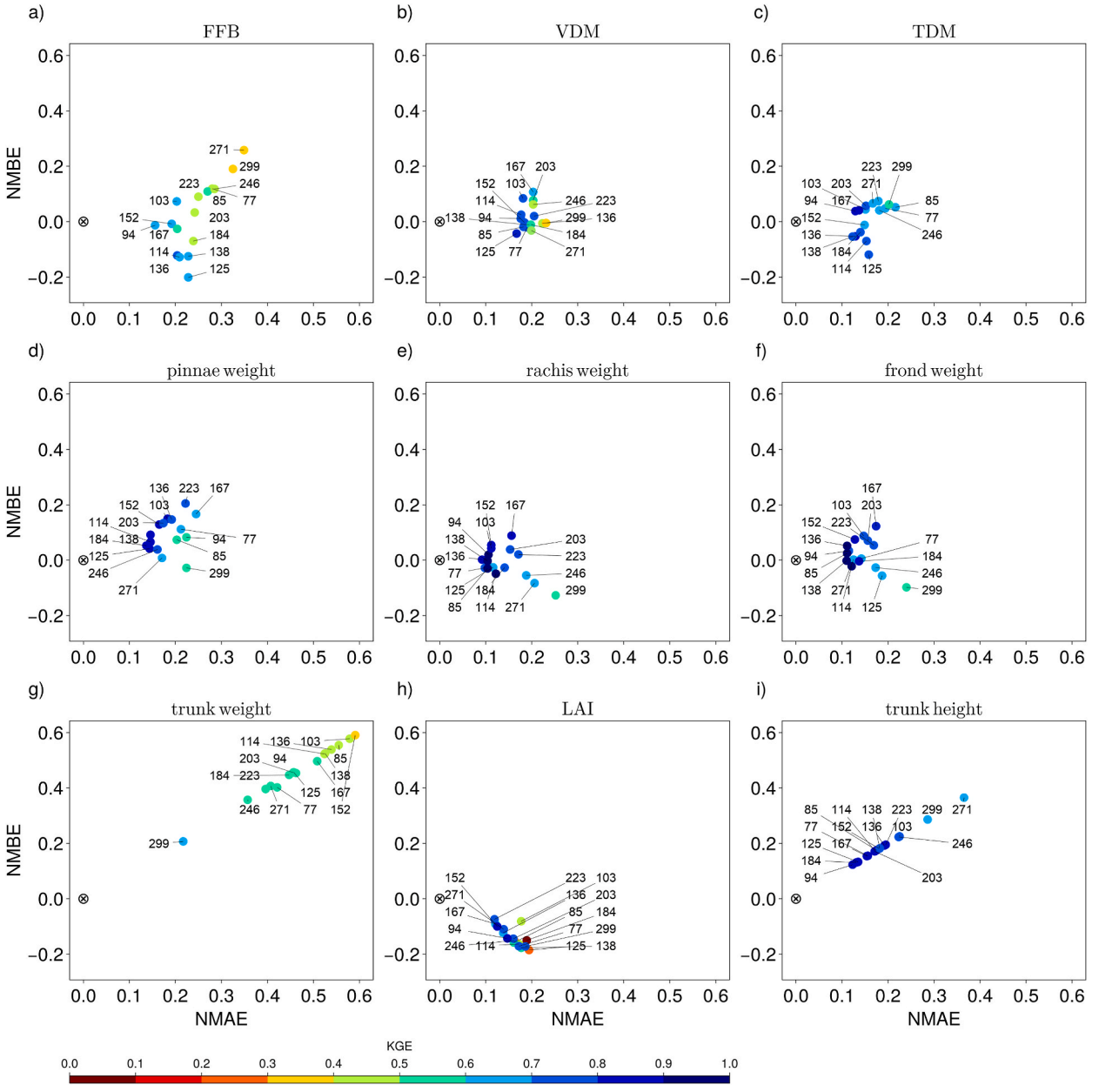

Fig. 17. Sg. Buloh: NMAE, NMBE, and KGE scores for each planting density (numeric labels on markers) for fresh fruit bunches (FFB) yield (a), vegetative dry matter (VDM) (b), total DM (TDM) (c), pinnae weight (d), rachis weight (e), frond weight (f), trunk weight (g), leaf area index (LAI) (h), and trunk height (i). Perfect simulations would have markers in the darkest blue (KGE = 1) and located at ⊗ position for NMAE = 0 and NMBE = 0.

highest planting densities (271 and 299 palms ha^{-1}) resulted in the largest errors (Fig. 17d–f). For Merlimau, simulations of leaf dry weight components (Figs. 10d-f and 11d-f) were more accurate with increasing planting density, particularly for mid-range planting densities (164–199 palms ha^{-1}) (Fig. 11d–f). The pinnae simulations were overestimated at lower planting densities (Fig. 11d).

Simulating trunk dry weight for all sites was challenging, with the model overestimating the weights for Kerayong and Sg. Buloh (Figs. 8g, 9g, 16g, and 17g) and underestimating that for Rengam and Sabrang (Fig. 12g-15g). For Merlimau, simulations (Figs. 10g–11g) were accurate for mid-range planting densities (181–220 palms ha^{-1}), but there was a tendency to underestimate and overestimate at smaller and higher planting densities, respectively (Fig. 11g). In contrast, trunk height simulations were accurate for all sites (Figs. 8i–15i), except for Rengam (Figs. 12i and 13i), and, to a smaller degree, Sg. Buloh (Figs. 16i–17i), where for these two sites, their trunk heights were overestimated.

The LAI was generally underestimated by a small bias of no more than −6% (Fig. 10h–17h and 18b and e), except for Kerayong,

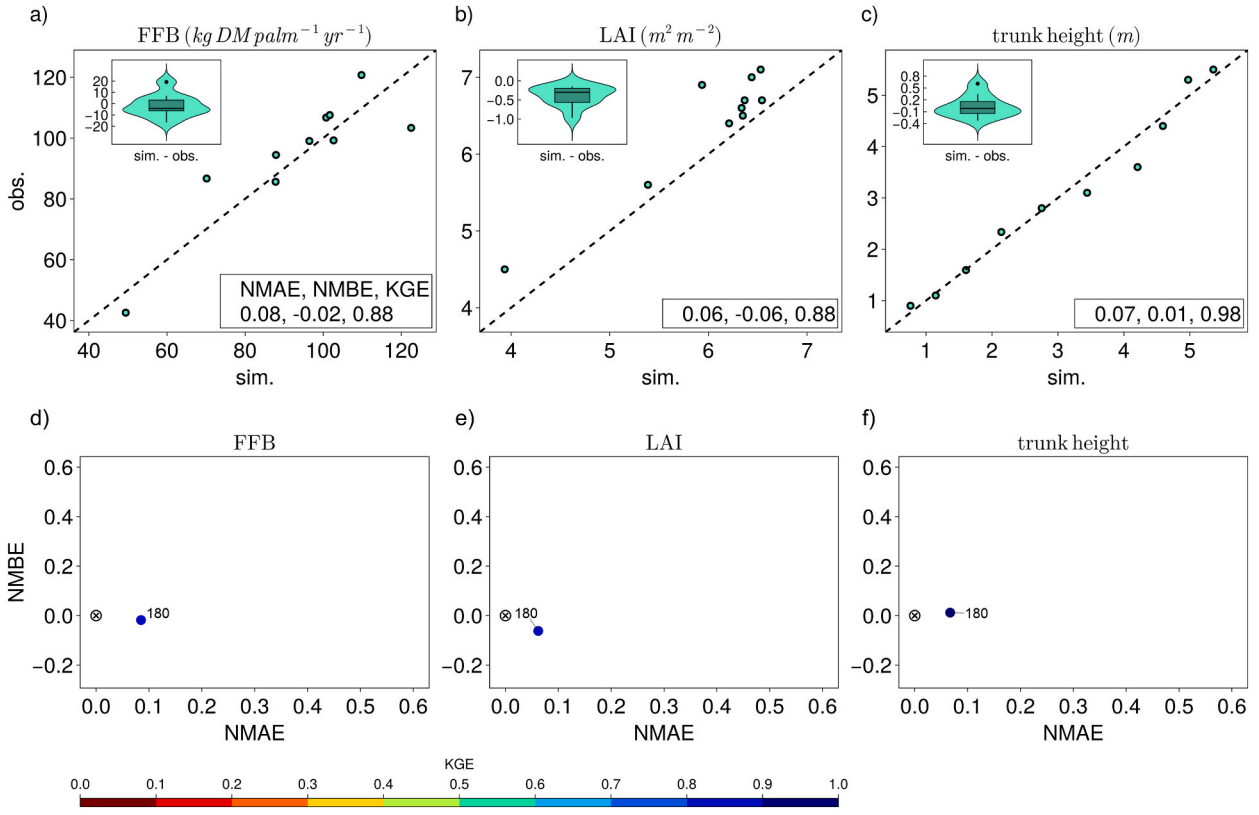

Fig. 18. Seri Intan: Upper panels show the agreement between observed (obs.) and simulated (sim.) values at 180 palms ha^{-1} for fresh fruit bunches (FFB) yield (a), leaf area index (LAI) (b), and trunk height (c). The inset box and violin plots show the distribution of model errors. The lower panels show the NMAE, NMBE, and KGE scores for FFB yield (d), LAI (e), and trunk height (f) (planting density of 180 palms ha^{-1} indicated on the markers). Perfect simulations would have markers in the darkest blue (KGE = 1) and located at ⊗ position for NMAE = 0 and NMBE = 0.

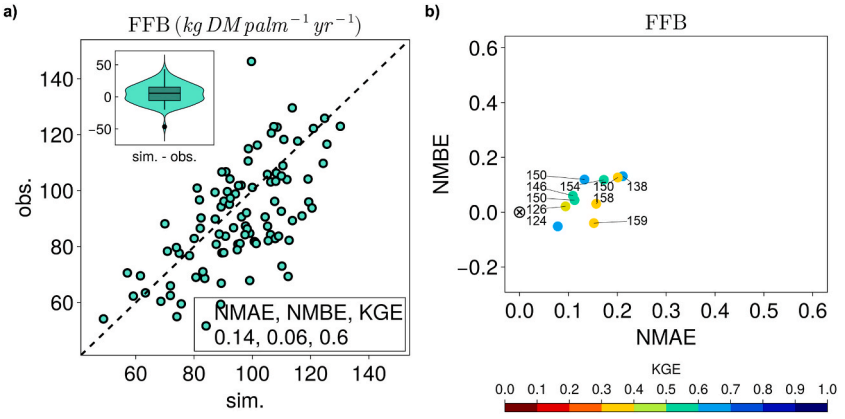

Fig. 19. Kalumpong: Agreement between observed (obs.) and simulated (sim.) values for fresh fruit bunches (FFB) yield for all planting densities (inset box and violin plots show the distribution of model errors) (a), and NMAE, NMBE, and KGE scores for every planting density (numeric labels on markers) (b). Perfect simulations would have markers in the darkest blue (KGE = 1) and located at ⊗ position for NMAE = 0 and NMBE = 0.

which was overestimated by 9 %, particularly for high LAI values (Figs. 8h and 9h). KGE scores for LAI, however, were strong positives between 0.78 and 0.92. Simulations for Sg. Buloh underestimated LAI for younger palms (<10 years) at low planting densities (≤125 palms ha^{-1}) (Supplementary Fig. S22-S25, panels o and p), whereas it was overestimated for mature trees (>10 years) at high planting densities (≥184 palms ha^{-1}) (Supplementary Fig. S29-S33, panels o and p).

Fig. 20 displays the distribution of scores for each of the three goodness-of-fit indices across all planting densities and sites. For yield, three-quarters of its scores (*i.e.*, below quartile 3) were below 25 % for absolute errors (NMAE) (Fig. 20a), between −7 and +12

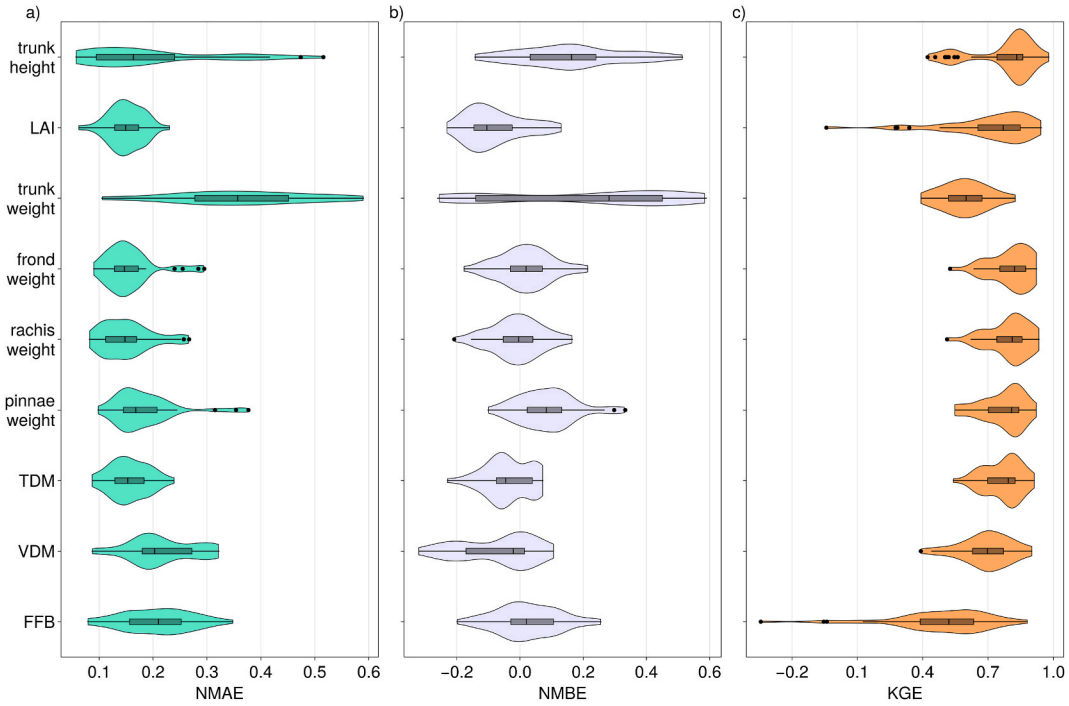

Fig. 20. Distribution of NMAE (a), NMBE (b), and KGE (c) scores for each simulated oil palm parameter across all planting densities and sites. Note: FFB is fresh fruit bunches yield, VDM and TDM are vegetative and total dry matter production, respectively, and LAI is leaf area index.

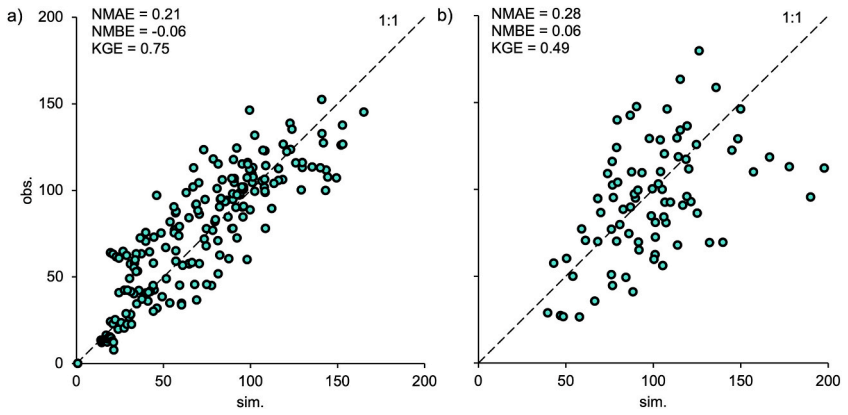

Fig. 21. Agreement between oil palm yield simulations (sim.) and observations (obs.) for all sites during El Niño (a) and La Niña (b) periods. NMAE, NMBE, and KGE are goodness-of-fit indices.

% for model biases (NMBE) (Fig. 20b), and between 0.39 and 0.88 for KGE scores (Fig. 20c) but with heavy skew to the left, caused by the four large errors at Merlimau's higher planting densities (≥220 palms ha^{-1}) (Fig. 11a).

As revealed earlier, trunk dry weight simulations were the most challenging. Its scores exhibited the largest variability, with three-quarters of the absolute errors between 10 and 45 % and model biases between −18 and + 52 % (Fig. 20a–c). Nonetheless, the KGE scores were largely not penalized, with three-quarters of the scores between 0.52 and 0.83. As previously mentioned, the KGE assesses a model by examining the linear correlation and similarity in both the mean and variability of two datasets (*e.g.*, between simulations and observations). Although there were large absolute errors and biases in the simulations of trunk dry weight, the moderate to high positive KGE scores indicated that the simulations and observations had a moderately strong correlation and comparable variability.

In contrast to trunk weight, trunk height simulations were accurate for most sites, displaying high positive KGE scores and very small model biases and absolute errors (Figs. 8i–11i, 14i, 15i, and 18c and f). The exceptions were Rengam (Fig. 12i and 13i), and to a lesser degree, Sg. Buloh (Figs. 16i and 17i), which explained the right- and left-skewed distributions of the NMAE and KGE scores, respectively.

Leaf dry weight components (pinnae, rachis, and fronds), LAI, and TDM showed similar distributions of model errors and KGE

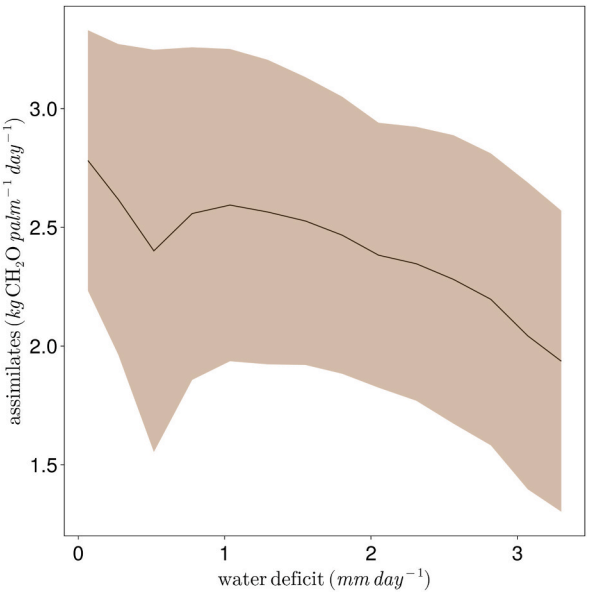

Fig. 22. Relationship between mean (solid line) daily water deficit and daily photosynthetic assimilate production. The shaded bands represent ±1 SD.

scores. They had KGE scores above 0.7 and three-quarters of the absolute errors were below 21 %, and model biases were between −12 and + 17 %. The KGE scores for LAI were strong positives, with three-quarters of their scores between 0.65 and 0.95, but there was a pronounced right skew due to a few outliers from Sg. Buloh's very low planting densities (≤94 palms ha^{-1}) (Fig. 17d). The VDM simulations presented slightly higher errors and weaker KGE scores than did the TDM simulations.

Overall, three-quarters of the metric scores ranged from 6 to 27 % for the model absolute errors, −22 to +17 % for the model bias, and 0.39 to 0.98 for the KGE (note: these ranges excluded metrics for the trunk weight simulations and the few outliers).

3.2. Water deficit

Yield simulations by Sawit.jl were responsive to El Niño and La Niña events, with yield simulations for El Niño periods (Fig. 21a) being more accurate than those for La Niña events (Fig. 21b). The study sites (Table 2) experienced strong El Niño events at least once in 1982–83, 1987–88, 1991–92, 1997–98, and 2015–16 and La Niña events in 1988–89, 1998–99, 2007–08, and 2010–11 [117]. During El Niño, the annual rainfall decreased by 5–24 %, with an average of 11 %. In contrast, La Niña caused an average rainfall increase of 16 %, ranging from 6 to 39 %. As a result of the lower rainfall, FFB yields declined by an average of 7 % during El Niño. Sites like Merlimau and Sg. Buloh experienced much larger drops of 29 % and 48 %, respectively. In contrast, higher rainfall due to La Niña saw yields increase by as much as 55 %, averaging 17 % for all sites. However, the impact of these events on oil palm yields varied across sites and planting densities, with some sites experiencing yield increases during El Niño events and decreases during La Niña events. Apart from the differences in rainfall, the impact of other weather variables, such as minimum and maximum air temperatures, solar radiation, and wind speed, on oil palm yields was not apparent because these meteorological factors did not exhibit noticeable changes during El Niño or La Niña years.

Yield simulations were more accurate for El Niño than for La Niña events. The tighter clustering of points along the 1:1 line in Fig. 21a compared to Fig. 21b, and the resulting higher KGE score (by 1.5 times) for El Niño, indicate a stronger correlation and greater similarity in variability between simulations and observations than that for La Niña.

Daily water deficit showed an inverse linear relationship with daily photosynthetic assimilate production (Fig. 22), with a roughly 200 g CH_2O $palm^{-1}$ day^{-1} decrease per 1 mm increase in daily water deficit. However, this relationship exhibited considerable variability. But this high variability is expected, as water deficit is just one of the numerous factors influencing photosynthesis. Three of these additional factors include maximum air temperature, total solar radiation, and the fraction of diffuse solar radiation (Fig. 23). The highest assimilate production occurred when the daily total solar radiation was between 11 and 19 MJ m^{-2} day^{-1}, diffuse radiation 60 and 80 %, and maximum air temperatures 27 and 33 °C.

Furthermore, the annual water deficit was linearly related to the FFB yield gap (percentage ratio of the measured yield to the simulated potential yield) (Fig. 24). Depending on the location, an increase of 100-mm in the annual water deficit resulted in a 1–9 % increase in the yield gap. Sites with coarse-textured soils, such as Merlimau and Rengam (Table 2), were more susceptible to higher water stress than sites with fine-textured soils, which was also evident from the nonlinear relationship between soil texture and annual water deficit (Fig. 25a). Interestingly, this chart shows that, as the soil texture becomes coarser, the water deficit initially increases rapidly for fine-textured soils (*dg* below 3 μm), and then the rate of increase gradually diminishes as the texture becomes even coarser.

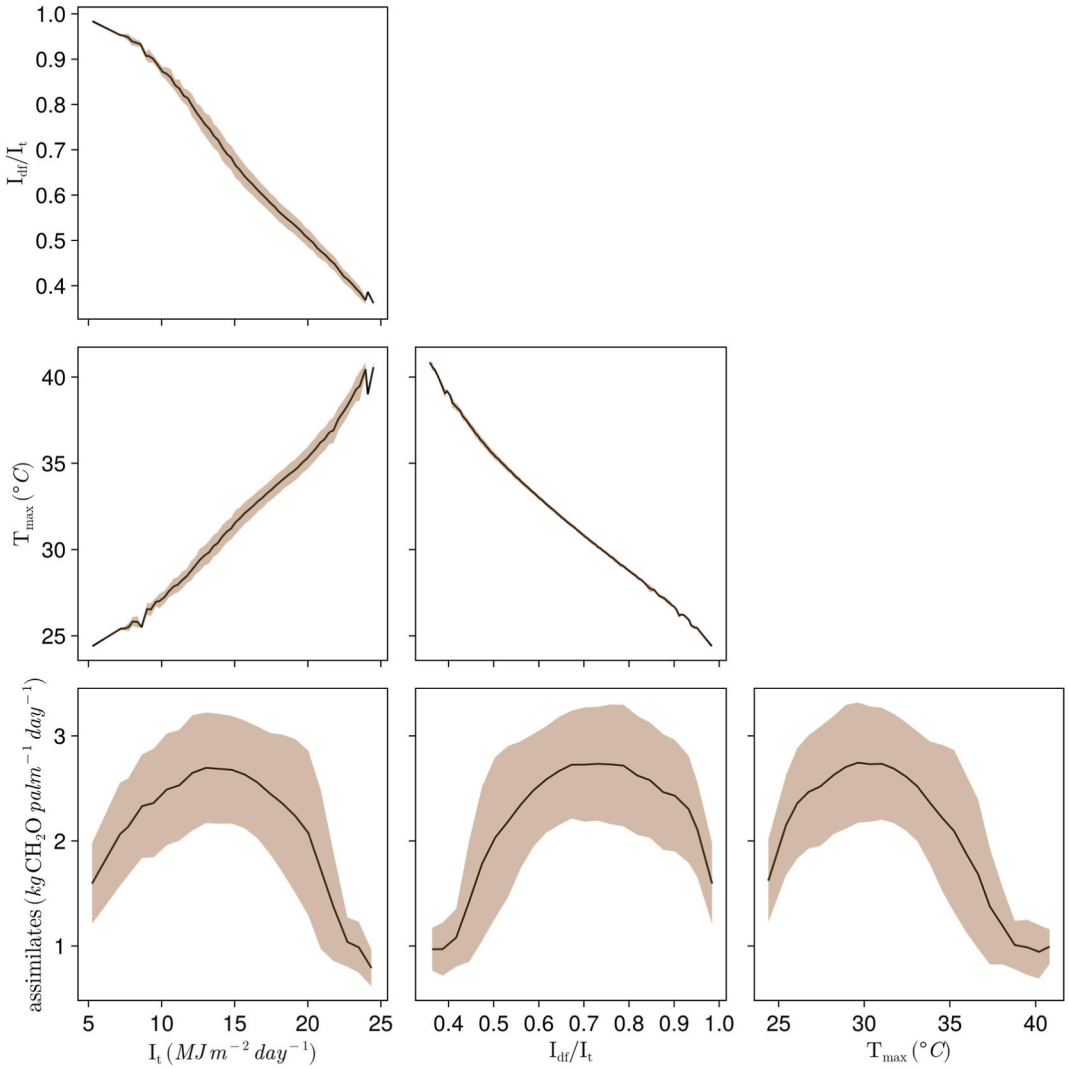

Fig. 23. Relationship between mean (solid line) daily production of assimilates (via photosynthesis) with daily values of total solar radiation (I_t), its proportion of diffuse solar component (I_{df}/I_t), and maximum air temperature (T_{max}). The shaded bands represent ±1 SD.

Finally, the annual water deficit had an inverse linear relationship with the annual rainfall, with sites with lower rainfall experiencing higher annual water deficits (Fig. 25b). Roughly, every 100-mm decline in annual rainfall would result in a 14 mm yr^{-1} increase in the annual water deficit.

4. Discussion

Sawit.jl was specifically developed for Malaysia's climate characteristics. It considers a wide range of planting densities and soil textures, unlike other oil palm models, *e.g.*, Refs. [10,16,43]. Furthermore, Sawit.jl does not use any radiation use efficiency functions but instead relies on local weather and environmental conditions to determine photosynthesis and ultimately yield. Sawit.jl also does not require pre-existing vegetative information, such as annual dry matter production, leaf area index, or standing vegetative biomass [10,43].

However, this model requires site-specific data on instantaneous weather properties (*e.g.*, air temperature, wind speed, and air vapor pressure) and soil water characteristics (*e.g.*, saturation, field capacity, and permanent wilting point). Unfortunately, most of these data are often not readily available for many oil palm growing areas in Malaysia. To address this, Sawit.jl uses equations that have been validated for local Malaysian weather and soil conditions to simulate the necessary information [52,98,110]. Sawit.jl additionally considers the influence of soil texture on soil water availability to oil palm, a feature not present in most other oil palm models. As a result, compared to models such as OPSIM, SIMPALM, and PALMSIM, Sawit.jl better accounts for the effects of weather factors such as air temperature, solar radiation, vapor pressure deficit, wind speed, and rainfall, as well as soil texture and water

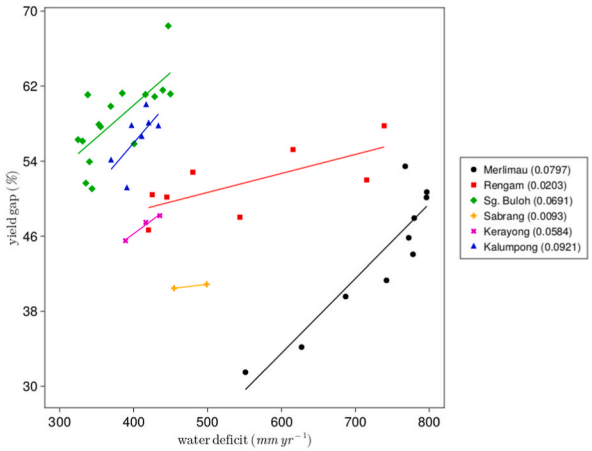

Fig. 24. Increase in mean yield gap with annual water deficit for mature oil palms (≥10 yrs) at 130–150 palms ha^{-1} across all sites (Seri Intan was excluded because this site had only one planting density of 180 palms ha^{-1}). Values in brackets in the legend indicate the slopes of the fitted linear regression lines.

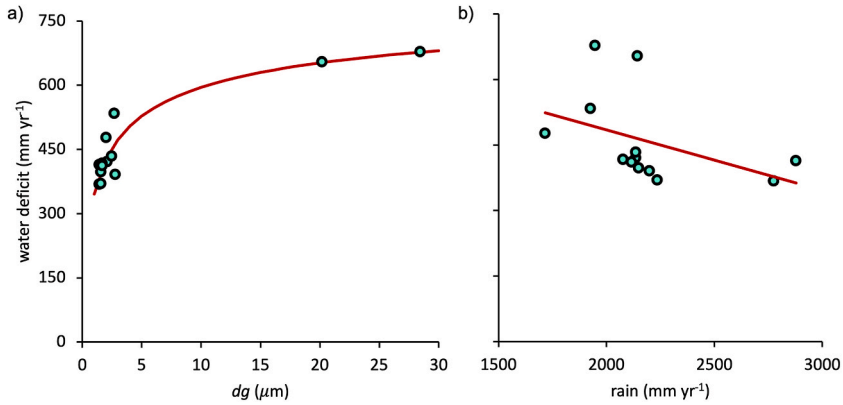

Fig. 25. Relationship between annual water deficit with soil texture (a) and annual rainfall (b). Soil texture is represented by *dg*, which is the geometric mean diameter of the soil's three primary particle sizes, such that increasing *dg* values indicate that soils have increasingly more sand and less clay [89].

retention characteristics, on oil palm growth simulations.

Sawit.jl was also specifically developed to simulate the growth and yield of oil palm across a wide range of densities, allowing it, for instance, to determine the ideal planting density for a particular environment. Planting density is a crucial management approach for optimizing palm oil production [44,45]. Consequently, Sawit.jl can potentially map oil palm yields in Peninsular Malaysia. Although Hoffman et al. [16] reported PALMSIM's ability to simulate yield for expansive areas in Malaysia and Indonesia, PALMSIM simulations are restricted to high-rainfall environments, as they cannot simulate water-limited yields. In contrast, Sawit.jl has been parameterized to simulate yield under existing weather conditions, which is vital for the accurate yield gap analysis of oil palm. However, as shown in Fig. 21, Sawit.jl produced more accurate results for drier than wetter weather conditions.

Sawit.jl's accuracy varied depending on the site, planting density, and oil palm parameter being simulated. Overall, the simulations were accurate for aspects such as vegetative and total dry matter production, standing rachis and frond biomass, and trunk height, as evidenced by their low NMAE values, large positive KGE values, and near-zero NMBE values (Fig. 20a–c).

However, yield simulations can be improved by more accurately accounting for the sensitivity of fruit bunch production to changes in growth conditions [106,118–121]. Sawit.jl attempted to account for this by including a parameter that represents the genetic predisposition to produce female flowers and the probability of deciding whether female flowers would be aborted by water stress (Eq. (38)). However, the limited understanding and research on the interaction between the oil palm genotype and environment is likely to have contributed to the occasional inaccuracies of Sawit.jl, as this interaction is not thoroughly or adequately represented in the model. Consequently, Sawit.jl has not been parameterized to account for yield fluctuations due to the flowering cycle and fruiting activity [118,122]. Increased fruiting activity can affect future yield components, amplify the yield cycle, and perpetuate a cycle that deviates from the simulated cycle. Fruiting activity was not sufficiently incorporated into Sawit.jl because there is no known simple physiological response of the oil palm to it.

Sawit.jl was initially designed for level 2 crop production, focusing solely on the limitations imposed by climate and water availability [55]. Enhancing the model to encompass level 3 crop production by integrating the factors of nutrient availability and uptake would significantly enhance its accuracy.

Overestimated trunk weights in Kerayong, Sg. Buloh, and Sabrang possibly resulted from higher dry matter allocation to the trunk. The mean dry matter partitioning ratio of 0.17 reported by Cheah et al. [51] and used by Sawit.jl for all sites was higher than that 0.12 used by the OPSIM and PALMSIM models. Another possibility is that Sawit.jl's method of distributing assimilates within the trunk, which was based on van Kraalingen et al. [43], may not accurately reflect real field conditions. van Kraalingen et al. [43] observed that the upper trunk section (between the lowest leaf and trunk apex) had much higher tissue activity than the area below the lowest leaf (lower trunk section). Therefore, they hypothesized that the actively growing portion of the trunk was the upper section and that this section would be prioritized for receiving new assimilates. They further estimated the dry weight of the upper trunk section to be no more than 45 kg of the total trunk weight. It is unclear whether this holds true for all the study sites and whether Sawit.jl's higher trunk partitioning ratio contributed to the discrepancies observed in Sg. Buloh, Kerayong, and Sabrang. This suggests that a more robust method for partitioning trunk dry matter is required.

Both observations and simulations showed that oil palm yield was significantly influenced by planting density. As planting density increases, yield per palm decreases because of increased interpalm competition [44,45]. Sawit.jl can simulate this competition effect by predicting lower yields as planting density increases. However, considerable knowledge gaps remain regarding the impact of planting density on oil palm growth and yield, such as microclimate conditions within and beneath oil palm canopies. For example, little is known about the vertical wind speed profile above and below canopies or how soil water content and plant water uptake would vary with planting density. Additionally, a precise method for scaling up the leaf-to-canopy conductance requires further investigation. For some sites, Sawit.jl's prediction errors varied with planting density, suggesting that the model's characterization of microclimate conditions, particularly beneath very low and dense canopies, is not yet adequately representative. Quantifying the increase in interpalm competition for solar radiation and nutrients is likely to improve the model simulations for high planting densities. Further research is needed to determine the effects of planting density on dry matter and nutrient content partitioning among the individual oil palm tree components. A better understanding of these properties would allow oil palm models to more accurately represent the daily variability of microclimate conditions under oil palm canopies and generate yield predictions that closely match the observed yield fluctuations.

Yield simulations specifically for periods during El Niño and La Niña were also examined, as they would indicate whether the model was sensitive to the impact of water deficits (such as El Niño) and water gains (such as La Niña) on oil palm yield. Overall, yield simulations matched observations for both El Niño and La Niña, although simulations were more accurate for El Niño than for La Niña. Although El Niño brings lower precipitation and therefore decreases crop yields, certain El Niño events actually saw yields at some sites, such as Kerayong and Seri Intan, increasing by 11–12 %. Moreover, Merlimau experienced a lower decline in oil palm yield than Sg. Buloh during El Niño (29 % at Merlimau vs. 48 % at Sg. Buloh). This is despite Merlimau having a coarser textured soil than Sg. Buloh, and according to Figs. 24 and 25a, Merlimau should be more susceptible to higher water deficits than Sg. Buloh. This demonstrates that other environmental factors (such as rainfall distributions or patterns and atmospheric evaporative demand) or crop physiological factors can mitigate or conceal the negative effects of El Niño on oil palm yield. There is also a time lag of several months between the initiation of stress and its impact on yield [123]. This means that the impact of stress on oil palm may only emerge months after the stress has occurred. This physiology of oil palm adds complexity, making it difficult to isolate and quantify the effects of individual stress factors on oil palm. La Niña's impact, like El Niño's, also varied across different locations and planting densities. Although most sites experienced increased yields, some sites, such as Seri Intan and a few field blocks at Kalumpong, had yields declining by 9–10 %.

Water deficit is one factor among many influencing photosynthesis. Rising air temperatures, for example, increase vapor pressure deficits, which would reduce stomatal openings and photosynthesis, while also being associated with increased soil water loss and plant water stress [86,124,125]. However, apart from water deficit, this study observed that daily photosynthesis across the sites was more directly related to the daily values of maximum air temperature, total solar radiation, and the fraction of the diffuse component in the solar radiation (Fig. 23).

Photosynthesis is enhanced more by diffuse than direct solar radiation [126–128]. Direct radiation is incident on only one part of the canopy because this solar component arrives from a single direction, thus reaching only a fraction of the leaves in the canopy and leaving the rest in deep shade. This localized concentration of direct radiation easily saturates canopy photosynthesis and, in turn, reduces radiation use efficiency [126]. In contrast, the diffuse solar component, as it arrives from multiple directions, can penetrate deeper into the canopy and illuminate the canopy more evenly. Several studies, as reviewed by Kanniah et al. [129], have reported that plant productivity increased even when the total solar radiation decreased, provided that this decrease was accompanied by an increase in the proportion of diffuse solar component.

There is, however, a balance between total solar radiation and the ratio of diffuse to direct component for photosynthesis (Fig. 23). High total solar radiation (above 20 MJ m^{-2} day^{-1}) offered more energy, but photosynthesis remained limited by the smaller proportion of diffuse radiation. But at low total solar radiation (below 9 MJ m^{-2} day^{-1}), photosynthesis was instead limited by the low energy, despite having a higher proportion of diffuse radiation. The optimal balance for ideal oil palm growth was found to be 11–17 MJ m^{-1} day^{-1} of total solar radiation and a 60–80 % diffuse component, corresponding to maximum air temperatures of 27–33 °C, which is consistent with Corley and Tinker [42], who reported the ideal range to be 29–33 °C. They also reported that the ideal minimum air temperature range was 22–24 °C, which this study also observed (results not shown); however, compared with the maximum air temperature, relationships involving minimum air temperature across the seven sites were less distinct and weaker.

Attempts to relate the annual rainfall and FFB yields across the seven sites revealed no clear trend, unlike Tohiruddin et al. [130],

who observed a clear positive linear relationship between them across several oil palm plantations spanning North and South Sumatra, Indonesia. This discrepancy might be due to Sumatra's broader rainfall range (1500–4000 mm) compared with our study (1800–2800 mm). Aldrian and Susanto [131] further classified Indonesia as having three distinct climate rainfall variability regions, with North and South Sumatra belonging to separate regions because they have unique climate patterns and responses to the environment.

A clearer trend was instead found when the simulated annual water deficits were correlated with the FFB yield gaps (Fig. 24). Depending on the location, every increase by 100-mm in the annual water deficit would result in a 1–9 % rise in the yield gap. This range is not too different from that estimated by Carr [132], and Caliman and Southworth [133]: an 8–10 % increase in the FFB yield gap during the first year and a 3–4% increase in the second year, resulting from a 100-mm annual water deficit.

Sites with higher sand contents experienced greater water deficits than those with higher clay contents, which is consistent with observations by other researchers [134–136]. Water depletion in sandy soils occurs primarily through drainage or percolation, whereas clayey soils predominantly lose water through evaporation from the soil surface [90,137,138]. And as the soil surface progressively dries out because of evaporation, its surface resistance increases, making it increasingly difficult for further water to evaporate [89,139,140]. This means that the drying topsoil develops an increasingly resistant barrier against additional evaporative loss. As a result, fine-textured soils lose less water than coarse-textured soils. Additionally, coarse-textured soils have a lower water retention capacity than fine-textured soils, owing to their larger pores.

5. Conclusions

The Sawit.jl model showed overall good accuracy in simulating all oil palm parameters (except for trunk weight) across the seven study sites with diverse planting densities, soil textures, and local climates. Goodness-of-fit metrics mostly ranged from 6 to 27 % for model absolute errors, −22 to +17 % for model bias, and 0.38 to 0.98 for KGE. The model predicted oil palm yield response to sudden annual rainfall changes, such as those occurring during strong El Niño and La Niña events. It also accounts for the effects of soil texture, rainfall, and several meteorological factors on water deficits and crop photosynthesis. However, model accuracy varied by site, planting density, and the oil palm parameters being simulated. The model was also more accurate for drier weather conditions than for wetter weather conditions. The model could be improved by refining the dry matter partitioning mechanism for the trunk, introducing fruiting activity to better account for yield fluctuations, and characterizing the microclimate conditions beneath canopies more accurately, especially for very low- and high-density stands. Overall, Sawit.jl can effectively predict the effects of various weather conditions, soils, and planting densities on oil palm growth and yield, supporting more efficient plantation management and better decision-making in the local industry.

Data availability

The full source code for Sawit.jl is available for download from github.com/cbsteh/Sawit.jl.

Funding Statement

This research was funded by the Fundamental Research Grant Scheme (FRGS) no. FRGS/1/2022/WAB04/UPM/02/2 under the Ministry of Higher Education (KPT), Malaysia.

CRediT authorship contribution statement

Christopher Boon Sung Teh: Writing – review & editing, Writing – original draft, Visualization, Validation, Supervision, Software, Resources, Project administration, Methodology, Investigation, Funding acquisition, Formal analysis, Data curation, Conceptualization. **See Siang Cheah:** Writing – review & editing, Visualization, Validation, Supervision, Resources, Project administration, Methodology, Investigation, Formal analysis, Data curation, Conceptualization. **Harikrishna Kulaveerasingam:** Writing – review & editing, Resources, Formal analysis.

Declaration of competing interest

The authors declare that they have no known competing financial interests or personal relationships that could have appeared to influence the work reported in this paper.

Appendix A. Supplementary data

Supplementary data to this article can be found online at https://doi.org/10.1016/j.heliyon.2024.e32561.

References

[1] USDA Foreign Agricultural Service, in: Consumption of Vegetable Oils Worldwide from 2013/14 to 2022/2023, by Oil Type (In Million Metric Tons), 2023. https://www.statista.com/statistics/263937/vegetable-oils-global-consumption/. (Accessed 18 April 2023).

[2] Malaysian Palm Oil Board (MPOB), in: Overview of the Malaysian Oil Palm Industry 2021, Bangi, Malaysia, 2022. https://bepi.mpob.gov.my/images/overview/Overview2022.pdf.

[3] USDA Foreign Agricultural Service, in: Oilseeds: World Markets and Trade, 2023. https://apps.fas.usda.gov/psdonline/circulars/oilseeds.pdf.

[4] A.J. Challinor, C. Müller, S. Asseng, C. Deva, K.J. Nicklin, D. Wallach, E. Vanuytrecht, S. Whitfield, J. Ramirez-Villegas, A. Koehler, Improving the use of crop models for risk assessment and climate change adaptation, Agric. Syst. 159 (2018) 296–306, https://doi.org/10.1016/j.agsy.2017.07.010.

[5] S. Asseng, Y. Zhu, B. Basso, T. Wilson, D. Cammarano, K. Neal, Simulation modeling: applications in cropping systems A2- Alfen, in: Encyclopedia of Agriculture and Food Systems, Academic Press, Oxford, 2014, pp. 102–112. https://scholar.google.com/scholar?hl=en&as_sdt=0%2C5&q=simulation+modeling+applications+in+cropping+systems.

[6] C. Rosenzweig, J. Elliott, D. Deryng, A.C. Ruane, C. Müller, A. Arneth, K.J. Boote, C. Folberth, M. Glotter, N. Khabarov, K. Neumann, F. Piontek, T.A. Pugh, E. Schmid, E. Stehfest, H. Yang, J.W. Jones, Assessing agricultural risks of climate change in the 21st century in a global gridded crop model intercomparison, Proc. Natl. Acad. Sci. USA 111 (2014) 3268–3273, https://doi.org/10.1073/pnas.1222463110.

[7] A. Rival, Breeding the oil palm (Elaeis guineensis Jacq.) for climate change, Oilseeds & Fats, Crops and Lipids 24 (2017) 17, https://doi.org/10.1051/ocl/2017001.

[8] D.W.G. van Kraalingen, Simulation of Oil Palm Growth and Yield, Wageningen Agricultural University, 1985. Ph.D. Dissertation, https://wur.on.worldcat.org/search/detail/66885811?queryString=simulation+of+oil+palm+growth+and+yield.

[9] W. Gerritsma, Simulation of Oil Palm Yield, Wageningen Agricultural University, Wageningen, The Netherlands, 1988.

[10] E. Dufrêne, R. Ochs, B. Saugier, Oil palm photosynthesis and productivity linked to climatic factors, Oleagineux 45 (1990) 345–355.

[11] I.E. Henson, Modelling gas exchange, yield and conversion efficiency, in: Workshop on Productivity of Oil Palm, Palm Oil Research Institute of Malaysia, 1989. Bangi, Malaysia.

[12] I.E. Henson, Modelling the effects of 'haze' on oil palm productivity and yield, J Oil Palm Res 12 (2000) 123–134.

[13] I.E. Henson, OPFLSIM3 – an improved oil palm seasonal flowering and yield simulation model, Oil Palm Bulletin 53 (2006) 1–24. http://opb.mpob.gov.my/index.php/2020/03/29/opflsim3-an-improved-oil-palm-seasonal-flowering-and-yield-simulation-model/.

[14] I.E. Henson, Modelling dry matter production, partitioning and yield of oil palm. OPRODSIM: a mechanistic simulation model for teaching and research, in: Technical Manual and Users' Guide, Malaysian Palm Oil Board, Kuala Lumpur, 2009. http://myagric.upm.edu.my/id/eprint/8542.

[15] J.C. Combres, B. Pallas, L. Rouan, I. Mialet-Serra, J.P. Caliman, S. Braconnier, J.C. Soulié, M. Dingkuhn, Simulation of inflorescence dynamics in oil palm and estimation of environment-sensitive phenological phases: a model based analysis, Funct. Plant Biol. 40 (2012) 263–279, https://doi.org/10.1071/fp12133.

[16] M.P. Hoffmann, A. Castaneda Vera, M.T. Wijk, K.E. Giller, T. Oberthür, C. Donough, A.M. Whitbreadand, Simulating potential growth and yield of oil palm (Elaeis guineensis) with PALMSIM: model description, evaluation and application, Agric. Syst. 131 (2014) 1–10, https://doi.org/10.1016/j.agsy.2014.07.006.

[17] N.I. Huth, M. Banabas, P.N. Nelson, M.J. Webb, Development of an oil palm cropping systems model: lessons learned and future directions, Environ. Model. Software 62 (2014) 411–419, https://doi.org/10.1016/j.envsoft.2014.06.021.

[18] Y. Fan, O. Roupsard, M. Bernoux, G. Le Maire, O. Panferov, M.M. Kotowska, A. Knohl, A sub-canopy structure for simulating oil palm in the Community Land Model (CLM-Palm): phenology, allocation and yield, Geosci. Model Dev. (GMD) 8 (2015) 3785–3800, https://doi.org/10.5194/gmd-8-3785-2015.

[19] R.R.M. Paterson, L. Kumar, S. Taylor, N. Lima, Future climate effects on suitability for growth of oil palms in Malaysia and Indonesia, Sci. Rep. 5 (2015) 14457, https://doi.org/10.1038/srep14457.

[20] Y. Xu, P. Ciais, L. Yu, W. Li, X. Chen, H. Zhang, C. Yue, K. Kanniah, A.P. Cracknell, P. Gong, Oil palm modelling in the global land-surface model ORCHIDEE-MICT, Geosci. Model Dev. (GMD) 14 (2020) 4573–4592, https://doi.org/10.5194/gmd-14-4573-2021.

[21] A. Wu, Y. Song, E.J. Oosterom, G.L. Hammer, Connecting biochemical photosynthesis models with crop models to support crop improvement, Front. Plant Sci. 7 (2016) 1518, https://doi.org/10.3389/fpls.2016.01518.

[22] G.D. Farquhar, S. Caemmerer, J.A. Berry, A biochemical model of photosynthetic CO2 assimilation in leaves of C3 species, Planta 149 (1980) 78–90, https://doi.org/10.1007/BF00386231.

[23] G.T. Collatz, J.T. Ball, C. Grivet, J.A. Berry, Physiological and environmental - regulation of stomatal conductance, photosynthesis and transpiration: a model that includes a laminar boundary layer, Agric. For. Meteorol. 54 (1991) 107–136, https://doi.org/10.1016/0168-1923(91)90002-8.

[24] B.E. Medlyn, P. Berbigier, R. Clement, A. Grelle, D. Loustau, S. Linder, L. Wingate, P.G. Jarvis, B.D. Sigurdsson, R.E. McMurtrie, Carbon balance of coniferous forests growing in contrasting climates: model-based analysis, Agric. For. Meteorol. 131 (2005) 97–124, https://doi.org/10.1016/j.agrformet.2005.05.004.

[25] W. Cramer, A. Bondeau, F.I. Woodward, I.C. Prentice, R.A. Betts, V. Brovkin, P.M. Cox, V. Fisher, J.A. Foley, A.D. Friend, C. Kucharik, M.R. Lomas, N. Ramankutty, S. Sitch, B. Smith, A. White, C. Young-Molling, Global response of terrestrial ecosystem structure and function to CO2 and climate change: results from six dynamic global vegetation models, Global Change Biol. 7 (2001) 357–373, https://doi.org/10.1046/j.1365-2486.2001.00383.x.

[26] S. von Caemmerer, Biochemical Models of Leaf Photosynthesis, CSIRO Publishing, Collingwood, ON, 2000. https://doi.org/10.1071/9780643103405.

[27] B. Nugroho, Leaf Gas Exchange Measurement under Land Use Changes in Jambi, Indonesia, Ph.D. Dissertation, Georg-August-Universität Göttingen, 2018. https://uni-goettingen.de/de/document/download/d33ef53a3fc0dea840509ec8f43fefb9.pdf/MasterThesis_A07_Brainnditoyo_Nugroho.pdf.

[28] A. Meijide, A. Röll, Y. Fan, M. Herbst, N. Furong, F. Tiedemann, T. June, A. Rauf, D. Hölscher, A. Knohl, Controls of water and energy fluxes in oil palm plantations: environmental variables and oil palm age, Agric. For. Meteorol. 239 (2017) 71–85, https://doi.org/10.1016/j.agrformet.2017.02.034.

[29] K. Guan, B. Sultan, M. Biasutti, C. Baron, D. Lobell, Assessing climate adaptation options and uncertainties for cereal systems in West Africa, Agric. For. Meteorol. 232 (2015) 291–305, https://doi.org/10.1016/j.agrformet.2016.07.021.

[30] J.L. Monteith, Principles of Environmental Physics, Edward Arnold, London, 1973. https://archive.org/details/principlesofenvi0000mont/page/n3/mode/2up.

[31] C.M. Tfwala, A.G. Mengistu, I.B.U. Haka, L.D. Rensburg, C.C. Preez, Seasonal variations of transpiration efficiency coefficient of irrigated wheat, Heliyon 7 (2021) 6233, https://doi.org/10.1016/j.heliyon.2021.e06233.

[32] A.T.P. Bennie, L.D. Rensburg, M.G. Strydom, C.C. Preez. Response of crops on pre-programmed deficit irrigationWater Research Commission Report no. 423/1/97, 1997.

[33] A. Röll, F. Niu, A. Meijide, A. Hardanto, K. Hendrayanto, D. Hölscher, Transpiration in an oil palm landscape: effects of palm age, Biogeosciences 12 (2015) 5619–5633, https://doi.org/10.5194/bg-12-5619-2015.

[34] W.J. Shuttleworth, J.S. Wallace, Evaporation from sparse crops – an energy combination theory, Q. J. R. Meteorol. Soc. 111 (1985) 839–855, https://doi.org/10.1002/qj.49711146910.

[35] H. Yan, H. Oue, Application of the two-layer model for predicting transpiration from the rice canopy and water surface evaporation beneath the canopy, J. Agric. Meteorol. 67 (2011) 89–97, https://doi.org/10.2480/agrmet.67.3.1.

[36] Z. Iritz, L. Anders, H. Martti, G. Achim, E. Kellner, Test of a modified Shuttleworth–Wallace estimate of boreal forest evaporation, Agric. For. Meteorol. 98–99 (1999) 605–619, https://doi.org/10.1016/S0168-1923(99)00127-6.

[37] C.J. Vörösmarty, C.A. Federer, A.L. Schloss, Potential evaporation functions compared on US watersheds: possible implications for global-scale water balance and terrestrial ecosystem modeling, J. Hydrol. (Amst.) 207 (1998) 147–169, https://doi.org/10.1016/S0022-1694(98)00109-7.

[38] H.J. Farahani, W.C. Bausch, Performance of evapotranspiration models for maize: bare soil to closed canopy, Transactions of the ASAE 38 (1995) 1049–1059, https://doi.org/10.13031/2013.27922.

[39] F.W.T. Penning de Vries, The cost of maintenance processes in plant cells, Ann. Bot. 39 (1975) 77–92. https://edepot.wur.nl/218532.

[40] F.W.T. Penning de Vries, Respiration and growth, in: A.R. Rees, K.E. Cockshull, D.W. Hand, R.G. Hurd (Eds.), Crop Processes in Controlled Environments, Academic Press, Hand, 1972, pp. 327–346. https://edepot.wur.nl/218533.

[41] S.K. Ng, S. Thamboo, P. Souza, Nutrient contents of oil palms in Malaya. II Nutrients in vegetative tissues, Malays. Agric. J. 46 (1968) 332–391.
[42] R.H. V Corley, P.B. Tinker, The Oil Palm, fifth ed., Wiley Blackwell Publishing, Chichester, 2016. https://onlinelibrary.wiley.com/doi/book/10.1002/9781118953297.
[43] D.W.G. van Kraalingen, C.J. Breure, C.J.T. Spitters, Simulation of oil palm growth and yield, Agric. For. Meteorol. 46 (1989) 227–244, https://doi.org/10.1016/0168-1923(89)90066-X.
[44] T. Palat, N. Chayawat, R.H. V Corley, Maximising oil palm yield by high density planting and thinning, Planter 88 (2012) 241–256.
[45] M. Nazeeb, M.K. Tang, S.G. Loong, S.S. Barakbah, Variable density plantings for oil palm (Elaies guineensis) in Peninsular Malaysia, J Oil Palm Res (2008) 61–90.
[46] C.J. Breure, The effect of different planting densities on yield trends in oil palm, Exp. Agric. 24 (1988) 37–52, https://doi.org/10.1017/S0014479700015684.
[47] R.H. V Corley, Effects of plant density on growth and yield of oil palm, Exp. Agric. 9 (1973) 169–180, https://doi.org/10.1017/S0014479700005639.
[48] C.J. Breure, Rate of leaf expansion: a criterion for identifying oil palm (Elaeis guineensis Jacq.) types suitable for planting at high densities, NJAS - Wageningen J. Life Sci. 57 (2010) 141–147, https://doi.org/10.1016/j.njas.2010.03.001.
[49] C.J. Breure, T. Menendez, M.S. Powell, The effect of planting density on the yield components of oil palm (Elaeis guineensis Jacq, Exp. Agric. 26 (1990) 117–124, https://doi.org/10.1017/S0014479700015453.
[50] C.J. Breure, R.H. V Corley, Selection of oil palms for high density planting, Euphytica 32 (1983) 177–186, https://doi.org/10.1007/BF00036878.
[51] S.S. Cheah, S.A.A. Wahid, C.B.S. Teh, Standing biomass, dry matter production, and nutrient demand of tenera oil palm, Agronomy 12 (2022) 426, https://doi.org/10.3390/agronomy12020426.
[52] S.S. Cheah, C.B.S. Teh, M.R. Ismail, M.R. Yusop, Modelling hourly air temperature, relative humidity and solar irradiance over several major oil palm growing areas in Malaysia, J Oil Palm Res 32 (2020) 34–49, https://doi.org/10.21894/jopr.2020.0010.
[53] S.S. Cheah, C.B.S. Teh, Parameterization of the Farquhar-von Caemmerer-Berry C3 photosynthesis model for oil palm, Photosynthetica 58 (2020) 769–779, https://doi.org/10.32615/ps.2020.020.
[54] J. Bezanson, A. Edelman, S. Karpinski, V.B. Shah, Julia: a fresh approach to numerical computing, SIAM Rev. 59 (2017) 65–98, https://doi.org/10.1137/141000671.
[55] C.T. de Wit, F.W.T. Penning de Vries, L'Analyse des systemes de production primaire [Analysis of primary production systems, Agric. Res. Rep. 918 (1982) 20–27.
[56] J.E. Ephrath, J. Goudriaan, A. Marani, Modelling diurnal patterns of air temperature, radiation, wind speed and relative humidity by equations from daily characteristics, Agric. Syst. 51 (1996) 377–393, https://doi.org/10.1016/0308-521X(95)00068-G.
[57] J. Goudriaan, H.H. van Laar, Modeling potential crop growth processes. A textbook with exercise. Current Issues in Production Ecology, Kluwer Academic, Netherlands, 1994. https://archive.org/details/modellingpotenti0000goud.
[58] T. Khatib, A. Mohamed, K. Sopian, M. Mahmoud, Solar energy prediction for Malaysia using artificial neural networks, Int. J. Photoenergy 2012 (2012) 1–16, https://doi.org/10.1155/2012/419504.
[59] F.A. Dimas, S.I.H. Gilani, M.S. Aris, Hourly solar radiation estimation using ambient temperature and relative humidity data, Int. J. Environ. Sustain Dev. 2 (2011) 188–193, https://doi.org/10.7763/IJESD.2011.V2.122.
[60] G.G. Wilkerson, J.W. Jones, K.J. Boote, K.T. Ingram, J.W. Mishoe, Modeling soybean growth for crop management, Transactions of the ASAE 26 (1983) 63–73, https://doi.org/10.13031/2013.33877.
[61] K. Sopian, M.Y. Hj Othman, A. Wirsat, The wind energy potential of Malaysia, Renew. Energy 6 (1995) 1005–1016, https://doi.org/10.1016/0960-1481(95)00004-8.
[62] G.S. Campbell, J.M. Norman, An Introduction to Environmental Biophysics, second ed., Springer-Verlag, New York, 1998. https://doi.org/10.1007/978-1-4612-1626-1.
[63] J. Goudriaan. Crop micrometeorology: a simulation study, Simulation Monograph, Pudoc, Wageningen, 1977. https://edepot.wur.nl/166537.
[64] C.B.S. Teh, Introduction to Mathematical Modeling of Crop Growth. How the Equations Are Derived and Assembled into a Computer Program, Brown Walker Press, Boca Raton, Florida, USA, 2006. https://www.universal-publishers.com/book.php?book=1581129998.
[65] R. Lemeur, B.L. Blad, A critical review of light models for estimating the shortwave radiation regimes of plant canopies, Agric. Meteorol. 14 (1974) 255–286, https://doi.org/10.1016/0002-1571(74)90024-7.
[66] X. Yin, H.H. van Laar, Crop systems dynamics, in: An Ecophysiological Simulation Model for Genotype-By-Environment Intreactions, Wageningen Academic Publishers, The Netherlands, 2005. https://research.wur.nl/en/publications/crop-systems-dynamics-an-ecophysiological-simulation-model-for-ge.
[67] S.P. Long, C.J. Bernacchi, Gas exchange measurements, what can they tell us about the underlying limitations to photosynthesis? Procedures and sources of errors, J. Exp. Bot. 54 (2003) 2393–2401, https://doi.org/10.1093/jxb/erg262.
[68] C.J. Bernacchi, E.L. Singsaas, C. Pimentel, A.R. Portis Jr., S.P. Long, Improved temperature response functions for models of Rubisco-limited photosynthesis, Plant Cell Environ. 24 (2001) 253–259, https://doi.org/10.1111/j.1365-3040.2001.00668.x.
[69] C.J. Bernacchi, A.R. Portis Jr., H. Nakano, S. Caemmerer, S.P. Long, Temperature response of mesophyll conductance. Implication for the determination of Rubisco enzyme kinetics and for limitations to photosynthesis in vivo, Plant Physiol. 130 (2002) 1992–1998, https://doi.org/10.1104/pp.008250.
[70] T.D. Sharkey, What gas exchange data can tell us, Plant Cell Environ. 39 (2015) 1161–1163, https://doi.org/10.1111/pce.12641.
[71] T.D. Sharkey, C.J. Bernacchi, G.D. Farquhar, E.L. Singsaas, Fitting photosynthetic carbon dioxide response curves for C3 leaves, Plant Cell Environ. 30 (2007) 1035–1040, https://doi.org/10.1111/j.1365-3040.2007.01710.x.
[72] W. Brutsaert, Evaporation into the Atmosphere. Theory, History and Applications, D. Reidel Publishing Company, Dordrecht, The Netherlands, 1982. https://doi.org/10.1007/978-94-017-1497-6.
[73] S. Ortega-Farias, R. Antonioletti, A. Olioso, Net radiation model evaluation at an hourly time step for mediterranean conditions, Agronomie 20 (2000) 157–164, https://doi.org/10.1051/agro:2000116.
[74] Z. Su, T. Schmugge, W.P. Kustas, W.J. Massman, An evaluation of two models for estimation of the roughness height for heat transfer between the land surface and the atmosphere, J. Appl. Meteorol. 40 (2001) 1933–1951, https://doi.org/10.1175/1520-0450.
[75] W.P. Kustas, J.M. Norman, Evaluation of soil and vegetation heat flux predictions using a simple two-source model with radiometric temperatures for partial canopy cover, Agric. For. Meteorol. 94 (1999) 13–29, https://doi.org/10.1016/S0168-1923(99)00005-2.
[76] W.J. Massman, An analytical one-dimensional model of momentum transfer by vegetation of arbitrary structure, Boundary-Layer Meteorol. 83 (1997) 407–421, https://doi.org/10.1023/A:1000234813011.
[77] G. Szeicz, I.F. Long, Surface resistance of crop canopies, Water Resour. Res. 5 (1969) 622–633, https://doi.org/10.1029/WR005i003p00622.
[78] W.J. Massman, A comparative study of some mathematical models of the mean wind structure and aerodynamic drag of plant canoipies, Boundary-Layer Meteorol. 40 (1987) 179–197, https://doi.org/10.1007/BF00140075.
[79] F. V Hansen, Surface Roughness Lengths, 1993. https://apps.dtic.mil/sti/tr/pdf/ADA274550.pdf.
[80] V. Rao, N. Rajanaidu, A. Kushairi, S. Jalani, Density effect in the oil palm, in: Proceedings in the ISOP International Workshop of Yield Potential in the Oil Palm, International Society for Oil Palm Breeders and PORIM, Bangi, 1992, pp. 71–79.
[81] B.J. Choudhury, J.L. Monteith, A four-layer model for the heat budget of homogeneous land surfaces, Q. J. R. Meteorol. Soc. 114 (1988) 373–398, https://doi.org/10.1002/qj.49711448006.
[82] H.J. Farahani, L.R. Ahuja, Evapotranspiration modeling of partial canopy/residue-covered fields, Transactions of the ASAE 39 (1996) 2051–2064, https://doi.org/10.13031/2013.27708.
[83] L. Shen, Z. Chen, Critical review of the impact of tortuosity on diffusion, Chem. Eng. Sci. 62 (2007) 3748–3755, https://doi.org/10.1016/j.ces.2007.03.041.
[84] J. Kallarackal, P. Jeyakumar, S.J. George, Water use of irrigated oil palm at three different arid locations in Peninsular India, J Oil Palm Res 16 (2004) 45–53.
[85] M.J. Kropff, Mechanisms of competition for light, in: M.J. Kropff, H.H. van Laar (Eds.), Modelling Crop–Weed Interactions, CAB International (in association with International Rice Research Institute), Wallingford, 1993, pp. 33–61. https://edepot.wur.nl/108849.

[86] E. Dufrêne, B. Saugier, Gas exchange of oil palm in relation to light, vapour pressure deficit, temperature and leaf age, Funct. Ecol. 7 (1993) 97–104, https://doi.org/10.2307/2389872.

[87] I. Pradiko, S. Rahutomo, R. Farrasati, E.N. Ginting, F. Hidayat, M. Syarovy, Transpiration of oil palm (Elaeis guineensis Jacq.) based on sap flow measurement: the relation to soil and climate variables, J Oil Palm Res 35 (2023) 168–184.

[88] G.S. Campbell, Soil physics with basic transport models for soil–plant systems, in: Developments in Soil Science, 14, Elsevier Science B.V, Amsterdam, The Netherlands, 1994. https://doi.org/10.1016/s0166-2481%2808%29x7009-6.

[89] M. Bittelli, G.S. Campbell, F. Tomeu, Soil Physics with Python. Transport in the Soil-Plant-Atmosphere System, Oxford University Press, Oxford, 2015, https://doi.org/10.1093/acprof:oso/9780199683093.001.0001.

[90] K.E. Saxton, W.J. Rawls, Soil water characteristic estimates by texture and organic matter for hydrologic solutions, Soil Sci. Soc. Am. J. 70 (2006) 1569–1578, https://doi.org/10.2136/sssaj2005.0117.

[91] T. Miyazaki, Water Flow in Soils, second ed., CRC Press, Boca Raton, 2005 https://doi.org/10.1201/9781420030136.

[92] P.N. Nelson, M. Banabas, D.R. Scotter, M.J. Webb, Using soil water depletion to measure spatial distribution of root activity in oil palm (Elaeis guineensis Jacq.) plantations, Plant Soil 286 (2006) 109–121, https://doi.org/10.1007/s11104-006-9030-6.

[93] Y. Farmanta, Analyses of rainfall interception in immature and mature oil palm plantation, in: M.P. Margarettha, S. Wiwaha Anas, S.P. Aras Melin (Eds.), Proceedings of International Seminar on the Land Reclamation Technology for Sustainable Land Use (IS-Lrt4slu), 2014, pp. 126–133. Jambi, Indonesia, https://www.academia.edu/12123588/Proceeding_International_Seminar_on_the_Land_Reclamation_Technology_for_Sustainable_Land_Use_IS_LRT4SLU_.

[94] H. van Keulen, N.G. Seligman, Simulation of water use, nitrogen and growth of a spring wheat crop. Simulation Monographs, Pudoc, Wageningen, 1987, https://doi.org/10.1017/S0014479700016902.

[95] F.S. Foong, Impact of moisture on potential evapotranspiration, growth and yield of oil palm, in: D. Arifin, K.W. Chan, S.R.S.A. Sharifah (Eds.), Proceedings of the 1999 PORIM International Palm Oil Conference, Agriculture, Palm Oil Research Institute of Malaysia, Kuala Lumpur, 1999, pp. 265–287. https://scholar.google.com/scholar?hl=en&as_sdt=0%2C5&q=F.S.+Foong%2C+Impact+of+moisture+on+potential+evapotranspiration%2C+growth+and+yield+of+oil%20+palm.

[96] H. Rey, P. Quencez, Dufrene, B. Dubos, Oil palm water profiles and water supplies in Côte d'Ivoire, Plantations, Recherche, Développement 5 (1998) 47–57.

[97] K.E. Saxton, W.J. Rawls, J.S. Romberger, R.I. Papendick, Estimating generalized soil water characteristics from texture, Soil Science Society of, America Journal 50 (1986) 1031–1035, https://doi.org/10.2136/sssaj1986.03615995005000040039x.

[98] C.B.S. Teh, J. Iba, Accuracy of the Saxton-Rawls method to estimate the soil water characteristics for minerals soils of Malaysia, Pertanika Journal of Tropical Agriculture 33 (2010) 297–302.

[99] C.T. de Wit, J. Goudriaan, H.H. van Laar, Simulation of Assimilation, Respiration and Transpiration of Crops, Pudoc, Wageningen, The Netherlands, 1978. https://edepot.wur.nl/167486.

[100] L.R. Hossner, Macronutrients, in: W. Chesworth (Ed.), Encyclopedia of Soil Science, Springer Netherlands, Dordrecht, 2008, pp. 443–445, https://doi.org/10.1007/978-1-4020-3995-9_337.

[101] N. Rajanaidu, A. Kushairi, Oil palm planting materials and their yield potential, in: Proceedings of the International Society of Oil Palm Breeders Symposium: Yield Potential in Oil Palm II, International Society of Oil Palm Breeders, Phuket, Thailand, 2006. https://scholar.google.com/scholar?hl=en&as_sdt=0%2C5&q=N.+Rajanaidu%2C+A.+Kushairi%2C+Oil+palm+planting+materials+and+their+yield+potential.

[102] J.C. Jacquemard, The Tropical Agriculturist: Oil Palm, Macmillan Education Ltd, London, 1998. https://scholar.google.com/scholar?hl=en&as_sdt=0%2C5&q=J.C.+Jacquemard%2C+The+Tropical+Agriculturist%3A+Oil+Palm.

[103] J.C. Jacquemard, Contribution to the study of the height growth of the stems of Elaeis guineensis Jacq, Study of the L2T x D10D cross, Oleagineux 34 (1979) 492–497.

[104] C.J. Breure, M.S. Powell, The one-shot method of establishing growth parameters in oil palm, in: H.A. Halim, P.S. Chew, B.J. Wood (Eds.), Proceedings of the 1987 International Oil Palm Conference. Progress and Prospects, Palm Oil Research Institute of Malaysia, Kuala Lumpur, 1988, pp. 203–209. https://scholar.google.com/scholar?hl=en&as_sdt=0%2C5&q=%09C.J.+Breure%2C+M.S.+Powell%2C+The+one%E2%80%90shot+method+of+establishing+growth+parameters+in+oil+palm.

[105] B.K.W. Kwan, The effect of planting density on the first fifteen years of growth and yield of oil palm in Sabah. Technical Bulletin No. 11, Department of Agriculture, Sabah, 1994. https://equip.sabah.gov.my/webopac/Record/0000282061/Similar.

[106] I.E. Henson, D. Mohd Tayeb, Physiological analysis of an oil palm density trial on a peat soil, J Oil Palm Res 15 (2003) 1–27. http://palmoilis.mpob.gov.my/publications/joprv15n2-henson.pdf.

[107] P.-A. Waite, B. Schuldt, R.M. Link, N. Breidenbach, T. Triadiati, N. Hennings, A. Saad, C. Leuschner, Soil moisture regime and palm height influence embolism resistance in oil palm, Tree Physiol. 39 (2019) 1696–1712, https://doi.org/10.1093/treephys/tpz061.

[108] I.E. Henson, S.H. Chai, Analysis of oil palm productivity. II. Biomass, distribution, productivity and turnover of the root system, Elaeis 9 (1997) 78–92.

[109] C. Jourdan, H. Rey, Architecture and development of the oil palm (Elaeis guineensis Jacq) root system, Plant Soil 189 (1997) 33–48. http://www.jstor.org/stable/42947948.

[110] C.B.S. Teh, S.S. Cheah, Modelling crop growth and yield in palm oil cultivation, in: A. Rival (Ed.), Achieving Sustainable Cultivation of Oil Palm. Introduction, Breeding and Cultivation Techniques, Burleigh Dodds Science, Publishing, Cambridge, UK, 2018, https://doi.org/10.4324/9781351114387.

[111] R.H. V Corley, M. Ng, C.R. Donough, Effects of defoliation on sex differentiation in oil palm clones, Exp. Agric. 31 (1995) 177–189.

[112] R.H. V Corley, J.J. Hardon, G.Y. Tan, Analysis of growth of the oil palm (Elaeis guineensis Jacq.) I. Estimation of growth parameters and application in breeding, Euphytica 20 (1971) 307–315, https://doi.org/10.1007/BF00056093.

[113] J.J. Hardon, W. C.N., I. Watson, Leaf area and yield in the oil palm in Malaya, Exp. Agric. 5 (1969) 25–32, https://doi.org/10.1017/S0014479700009935.

[114] C.J. Breure, The search for yield in oil palm: basic principles, in: T. Fairhurst, R. Härdter (Eds.), Oil Palm: Management for Large and Sustainable Yields, first ed., PPI/PPIC-IPI, Singapore, 2003, pp. 59–98. https://www.ipipotash.org/publications/publication-59.

[115] H. Kling, M. Fuchs, M. Paulin, Runoff conditions in the upper Danube basin under an ensemble of climate change scenarios, J. Hydrol. (Amst.) 424–425 (2012) 264–277, https://doi.org/10.1016/j.jhydrol.2012.01.011.

[116] J.M.W. Knoben, J.E. Freer, R.A. Woods, Technical note: inherent benchmark or not? comparing Nash–Sutcliffe and Kling–Gupta efficiency scores, Hydrol. Earth Syst. Sci. 23 (2019) 4323–4331, https://doi.org/10.5194/hess-23-4323-2019.

[117] National Oceanic Atmospheric Administration (NOAA), in: Cold & Warm Episodes by Season, 2023. https://origin.cpc.ncep.noaa.gov/products/analysis_monitoring/ensostuff/ONI_v5.php.

[118] R.H. V Corley, C.J. Breure, Fruiting activity, growth and yield of oil palm. I. Effects of fruit removal, Exp. Agric. 28 (1992) 99–109, https://doi.org/10.1017/S0014479700023048.

[119] R.H. V Corley, Effects of severe leaf pruning on oil palm, and its possible use for selection purposes, Malaysia Agriculture Research and Development Institute Research Bulletin 4 (1976) 23–28.

[120] C.J. Breure, Factors affecting yield and growth of oil palm teneras in West New Britain, Oleagineux 37 (1982) 213–227.

[121] R.H. V Corley, C.R. Donough, Potential yield of oil palm clones – the importance of planting density, in: V. Rao, I.E. Henson, N. Rajanaidu (Eds.), Proceedings of the Workshop on Yield Potential in the Oil Palm, International Society for Oil Palm Breeders, Kuala Lumpur, 1992, pp. 58–70. https://scholar.google.com/scholar?hl=en&as_sdt=0%2C5&q=%09R.H.+V+Corley%2C+C.R.+Donough%2C+Potential+yield+of+oil+palm+clones+%E2%80%93+the+importance+of+planting+density.

[122] C.J. Breure, R.H. V Corley, Fruiting activity, growth and yield of oil palm. II. Observations in untreated populations, Exp. Agric. 28 (1992) 111–121, https://doi.org/10.1017/S001447970002305X.

[123] H. Adam, M. Collin, F. Richaud, T. Beule, D. Cros, A. Omore, L. Nodichao, B. Nouy, J.W. Tregear, Environmental regulation of sex determination in oil palm: current knowledge and insights from other species, Ann. Bot. 108 (2011) 1529–1537, https://doi.org/10.1093/aob/mcr151.

[124] J.A. Bunce, Carbon dioxide effects on stomatal responses to the environment and water use by crops under field conditions, Oecologia 140 (2004) 1–10, https://doi.org/10.1007/s00442-003-1401-6.
[125] A. Tuzet, A. Perrier, R. Leuning, A coupled model of stomatal conductance, photosynthesis and transpiration, Plant Cell Environ. 26 (2003) 1097–1116, https://doi.org/10.1046/j.1365-3040.2003.01035.x.
[126] M.L. Roderick, G.D. Farquhar, S.L. Berry, I.R. Noble, On the direct effect of clouds and atmospheric particles on the productivity and structure of vegetation, Oecologia 129 (2001) 21–30, https://doi.org/10.1007/s004420100760.
[127] A. Knohl, D.D. Baldocchi, Effects of diffuse radiation on canopy gas exchange processes in a forest ecosystem, J Geophys Res Biogeosci 113 (2008), https://doi.org/10.1029/2007JG000663.
[128] P.B. Alton, P.R. North, S.O. Los, The impact of diffuse sunlight on canopy light-use efficiency, gross photosynthetic product, and net ecosystem exchange in three forest biomes, Global Change Biol. 13 (2007) 776–787, https://doi.org/10.1111/j.1365-2486.2007.01316.x.
[129] K.D. Kanniah, J. Beringer, P. North, L. Hutley, Control of atmospheric particles on diffuse radiation and terrestrial plant productivity: a review, Prog. Phys. Geogr. Earth Environ. 36 (2012) 209–237, https://doi.org/10.1177/0309133311434244.
[130] L. Tohiruddin, N.E. Prabowo, H.L. Foster, Comparison of the response of oil palm to fertilisers at different locations in North and South Sumatra, in: Proceedings of Agriculture Conference, International Oil Palm Conference (IOPC), Indonesian Oil Palm Research Institute, Bali, Indonesia, 2006, pp. 188–200. https://scholar.google.com.my/scholar?hl=en&as_sdt=0%2C5&q=L.+Tohiruddin%2C+N.E.+Prabowo%2C+H.L.+Foster%2C+Comparison+of+the+response+of+oil+palm+to+fertilisers+at+different+locations+in+North+and+South+Sumatra.
[131] E. Aldrian, R.D. Susanto, Identification of three dominant rainfall regions within Indonesia and their relationship to sea surface temperature, Int. J. Climatol. 23 (2003) 1435–1452, https://doi.org/10.1002/joc.950.
[132] M.K. V Carr, The water relations and irrigation requirements of oil palm (Elaeis guineensis): a review, Exp. Agric. 47 (2011) 629–652, https://doi.org/10.1017/S0014479711000494.
[133] J.P. Caliman, A. Southworth, Effect of drought and haze on the performance of oil palm, in: 1998 International Oil Palm Conference: Commodity of the Past, Today and the Future, Sept, Indonesian Oil Palm Research Institute and Indonesian Palm Oil Producers Association, Bali, 1998, pp. 23–25.
[134] L. Taiz, E. Zeiger, Plant Physiology, fifth ed., Sinauer Associates, Inc, Sunderland, 2010. https://scholar.google.com.my/scholar?hl=en&as_sdt=0%2C5&q=L.+Taiz%2C+E.+Zeiger%2C+Plant+physiology%2C+5th+ed.%2C+Sinauer+Associates%2C+Inc%2C+Sunderland%2C+2010.
[135] M. Farooq, A. Wahid, N. Kobayashi, D. Fujita, S.M.A. Basra, Plant drought stress: effects, mechanisms and management, Agron. Sustain. Dev. 29 (2009) 185–212, https://doi.org/10.1051/agro:2008021.
[136] M. Homaee, R.A. Feddes, C. Dirksen, Simulation of root water uptake. I. Non-uniform transient salinity using different macroscopic reduction functions, Agric. Water Manag. 57 (2002) 89–109, https://doi.org/10.1016/S0378-3774(02)00072-0.
[137] W.A. Jury, R. Horton, Soil Physics, sixth ed., John Wiley & Sons, 2004. https://scholar.google.com/scholar?hl=en&as_sdt=0%2C5&q=W.A.+Jury%2C+R.+Horton%2C+Soil+physics%2C+6th+ed.%2C+John+Wiley+%26+Sons%2C+2004.
[138] G.C. Topp, P.A. Ferre, Water content, in: J.H. Dane, G.C. Topp (Eds.), Methods of Soil Analysis, Part 4: Physical Methods, Soil Science Society of America, Madison, 2002, https://doi.org/10.2136/sssabookser5.4.c19.
[139] A. Amazirh, O.E.-R. Merlin, B. Salah, A. Chehbouni, Implementing a new texture-based soil evaporation reduction coefficient in the FAO dual crop coefficient method, Agric. Water Manag. 250 (2021) 106827, https://doi.org/10.1016/j.agwat.2021.106827.
[140] D. Or, J.M. Wraith, Temperature effects on soil bulk dielectric permittivity from the perspective of water content measurement: experimental results and hypothesis development, Water Resour. Res. 35 (1999) 361–369, https://doi.org/10.1029/1998WR900006.